ATOMISTIC SIMULATIONS AND MODELING OF DEFORMATION MECHANISMS IN ALUMINUM UNDER EXPERIMENTAL CONDITIONS

A Dissertation

Presented to the Faculty of the Graduate School

of Cornell University

in Partial Fulfillment of the Requirements for the Degree of

Doctor of Philosophy

by

Linh Duc Nguyen

January 2013

ATOMISTIC SIMULATIONS AND MODELING OF DEFORMATION MECHANISMS IN ALUMINUM UNDER EXPERIMENTAL CONDITIONS

Linh Duc Nguyen, Ph.D.

Cornell University 2013

Atomistic simulations have been widely used to study deformation mechanisms of plasticity in metals and alloys. While being very effective for illuminating the controlling mechanisms in detail, direct atomistic simulations have many limitations such as short timescales and small spatial scales, when used to study large systems. Those limitations emerge when one desires to study materials under conditions more typical of application. My research is aimed to address the short-timescales challenges in atomistic simulations with relevant indirect approaches. I explore dislocation problems in different systems using several approaches and figure out relevant approaches for the chosen problems by comparing their performance. First, I adapt MD to simulate dislocation nucleation in a small 2D fcc Al simulation box with a cylindrical nanovoid inside. This problem serves as a test problem to validate indirect approaches conducted. I show that a variational TST approach, with the support of the finite temperature string (FTS) method, predicts dislocation nucleation rates in accordance with direct MD simulations. The work provides energetics information to illuminate the free energy characteristics of the system that explain the errors of approaches to predicting nucleation expectation time. Second, I build bigger simulation cells to study problems of dislocation nucleation from a faceted surface and from spherical nanovoids of different sizes. The problems are studied at realistic timescales in a variational TST framework, exploiting the FTS meth-

ods. Dislocation nucleation from surface study can be related to the strength of sub-micron Al wires. From the results, I make predictions for maximum attainable strength of Al nanowires, and for the associated strain rate sensitivity. The study of dislocation nucleation from voids is relevant to studying void growth mechanisms. My results contribute to a long-standing debate regarding what are the controlling mechanisms in void growth. Third, I study the interaction between dislocation and nanometer-size coherent metastable precipitates. These precipitates serve as impeders to dislocation mobility and hence help enhance alloy strength. I show here that transition in such systems is so complex that a typical transition tube in FTS cannot be practically defined. However, we can use part of the information from FTS computation to employ another sampling method, the transition interface sampling (TIS), for obtaining reaction rates of events in the systems with errors within an order of magnitude.

BIOGRAPHICAL SKETCH

Linh Nguyen grew up in Dalat, a small highland city in the central part of Vietnam. He graduated from Thanglong High School in his hometown in 1998. He attended Vietnam National University, Hanoi (VNUH), majoring in of physics. He graduated in 2002, with a bachelor of science in physics, in the top 10% of students in his major in that school year. He worked for the Center for Materials Science, VNUH, as an experimental research assistant for 3 years, from September of 2002 through May of 2005. His research during this stage are focused on magnetic thin films. Linh started his graduate study at the School of Applied and Engineering Physics (AEP) at Cornell University in August 2005. He spent the summer of 2006 with Dr. John Silcox's group learning about electron microscopes. Then he joined Dr. Hassan Padamsee in the physics department to study niobium surfaces until May of 2008. In summer of 2008, he switched fields, joining Dr. Derek Warner in the School of Civil and Environmental Engineering to study the mechanics of materials at the atomic scale, using atomistic modeling and state of the art simulation techniques. In his spare time, Linh reads international politics and military news.

To the whole research group for a friendly research environment.

To my family for all your support.

ACKNOWLEDGEMENTS

I gratefully acknowledge support from Paul Hess at the Office of Naval Research (Grants No. N00014-08-1-0862 and No. N00014-10-1-0323). I am also grateful for partial funding from a fellowship granted by the Vietnam Education Foundation during the 2005-2006 and 2006-2007 academic years.

TABLE OF CONTENTS

LIST OF TABLES

LIST OF FIGURES

CHAPTER 1

INTRODUCTION

Studying long-timescales events, such as thermally activated processes, with traditional MD simulation is not possible. Thus, other more indirect approaches are needed to efficiently study the controlling deformation mechanisms of plasticity in metals and alloys. This dissertation presents my work, using different approaches and numerical algorithms, on three specific problems, to extend the timescales well beyond those that are accessible to traditional MD. The problems are meaningful to a wide range of engineering applications. All of them are studied in experimental conditions. The dissertation is organized chronologically based on the three projects that I have completed. The second and the third chapters represent published work. The last chapter will be submitted for review very soon. The bibliography for all chapters is included in the Bibliography section.

The second chapter, entitled "Atomistic predictions of dislocation nucleation with transition state theory," has been published in *Physical Review B*, as indicated in the chapter. This work details how the combined use of atomistic simulations and TST has enabled significant improvements in the prediction of dislocation nucleation from a 2D cylindrical nanovoid in an fcc Al crystal. Five TST versions, varying from the most simplified to more advanced, are investigated. The results obtained from direct MD simulations are used as the standard to judge the performance of the TST approaches. A variational TST approach is utilized using the finite temperature string (FTS) method. With the method, a transition path in configuration space is described by a set of Voronoi cells, the centers of which represent a series, called a string, of intermediate con-

figurations connecting an initial configuration with a final configuration. Sampling procedures in FTS, for a certain class of problems, allow detection of the most probable transition path and provide information about transition flux in and out for each cell along the string, based on which free energy profile of the transition can be calculated. This chapter also reports on the application of variational TST to study dislocation nucleation from a free surface under shear loads. It provides a prediction for the upper bound strength for Al nanowires, and strain rate sensitivities calculated at different rates.

The third chapter, also focused on fcc Al crystals, entitled "Improbability of Void Growth in Aluminum via Dislocation Nucleation under Typical Laboratory Conditions," has been published in *Physical Review Letters* as indicated in the chapter. This work's aim was to better illuminate the mechanisms of void growth in metals. It concentrates on dislocation nucleation from spherical nanovoids of different void sizes and at different shear loads, using the same variational TST framework as for the free surface case in the second chapter. By combining TST results with a continuum analytic model, the predictions are generalized for voids of any size. The results indicate that dislocation nucleation is extremely rare at laboratory conditions and, hence, not a controlling mechanism of void growth, regardless of void sizes, unless local stresses reach the gigapascal range. The results from free surface study are also mentioned in this work as a comparison to a limit case of the fitting model when voids are infinitely large. The results show strong agreement.

The fourth chapter, entitled "Computing the Rates of Transition in Precipitate Hardened Al-Cu Alloy," reports my recent work, which focused on the interaction between dislocations and small coherent precipitates. This prob-

lem is relevant for a popular class of hardened alloys used in the aerospace industry. The simulation cell is built small enough to enable studies to be conducted within a reasonable timeframe, yet retains the complex energetic landscape. This works shows that the FTS method with a typical reaction coordinate is not sufficient to study the interaction between a dislocation and a precipitate because of the complexity in the energy landscape. Specifically, the FTS method is unable to provide a free energy barrier of transition. Transition interface sampling (TIS), as an alternative approach, while lacking the ability to directly measure the free energy barrier, can predict expectation time of transitions with errors no larger than an order of magnitude. TIS was also developed to calculate the rate of rare events. But instead of constructing information for the whole transition based on the data obtained for segments of trajectory connecting neighbor cells, TIS calculates the frequency of occurrence of trajectories that start from an initial configuration, pass a certain interface and, finally, reach the next interface. Performing TIS for all of the pairs of interfaces along the set of interfaces allows calculation of the rate of transition from the initial to the final configuration.

CHAPTER 2

ATOMISTIC PREDICTIONS OF DISLOCATION NUCLEATION WITH TRANSITION STATE THEORY

By Linh D. Nguyen, Kristopher Baker and Derek H. Warner

As published in *Physical Review B* **84** (2011) 024118

2.1 Abstract

The combined use of atomistic simulations and transition state theory (TST) has enabled significant improvements in the prediction of thermally activated processes in a wide range of applications, e.g. conformation changes in molecules, chemical reactions, kinetic phase transitions and solid state diffusion. However, such an approach is still in its infancy with regard to mechanics of materials applications. Focusing here on dislocation nucleation in Al, we examine the utility of five TST-based approaches. Using the finite temperature string method, we interpret the success/failure of each approach in terms of a full energetic analysis of the nucleation processes. After showing that advanced TST approaches such as variational TST can accurately predict nucleation rates, we employ variational TST to study dislocation nucleation from a free surface under ordinary laboratory conditions. The predictions (1) demonstrate that nucleation will only occur under very high stresses at room temperature, (2) provide an upper bound on the shear strength of Al in dislocation starved contexts, and (3) provide a rate sensitivity signature of the nucleation process.

2.2 Introduction

A long-standing challenge associate with direct molecular dynamics (MD) simulations of plasticity is the discrepancy of timescales that exists between simulations and experiments. The brief nanosecond timescale of MD combined with the thermally activated nature of plasticity encourages simulations to be performed at high loads and/or temperatures relative to experiment to ensure that plastic deformation occurs within the simulation time domain. However, this strategy can skew the competition between deformation mechanisms and make interpretation of the simulation results relative to experiment difficult [90, 89].

To circumvent this challenge, the mechanics of materials community has begun to employ transition state theory (TST) approaches that utilize atomistically computed quantities as input. TST provides a framework for computing the rate at which thermally activated events will occur without directly performing the simulation [21]. Notable examples have included dislocation kink pair formation [67, 91, 34], dislocation cross-slip [86], dislocation nucleation from a crack tip [95, 22] and dislocation nucleation from free surfaces [94, 27, 25]. While these atomistic simulations have been pioneering in that they attempt to investigate deformation mechanisms under typical experimental conditions, the validity of the simplifying assumptions has never been analyzed. Here, we investigate dislocation nucleation from a cylindrical nanovoid using five TST-based approaches of varying accuracy, assumptions, and effort, and compare the predictions to direct MD simulation results. Our multipronged investigation not only seeks to identify approaches capable of accurately computing dislocation nucleation rates, it illuminates the energetics associated with thermally activated nucleation. After discovering that only the most advanced TST ap-

proaches can predict the rate of nucleation to within the same order of magnitude as direct MD simulation, we use variational TST to predict dislocation nucleation from a faceted surface. Considering that the interatomic potential used in this work has been shown to accurately predict athermal dislocation nucleation relative to electronic structure calculations [54], the predictions given here are likely the most accurate predictions of dislocation nucleation at ordinary experimental temperatures and time-scales to date.

While dislocation nucleation can play an important role in long-studied metallurgical processes such as crack growth [63, 64] and ductile failure [46, 45, 1, 10, 77], it is also relevant to more contemporary topics such as the deformation and strength of nano-dimensioned metals [14, 39]. Here we discuss our predictions of dislocation nucleation in the context of the latter. Specifically, our predictions provide an upper bound for the maximum strength of Al nanowires and an experimentally observable indicator of dislocation nucleation controlled deformation, i.e. a strain rate sensitivity.

2.3 Transition State Theory

Non-quantum TST theory is based on the idea that the rate at which an ergodic system transitions across a dividing surface partitioning configuration space can be exactly expressed as the average absolute value of the velocity of the system normal to the dividing surface weighted by the equilibrium probability that the system resides on the dividing surface [21, 15, 92, 32]. Accordingly, considering a dividing surface, $\mathscr{S}_D$, separating two regions a and b that partition the configuration space of an NVT system, the rate at which the system transitions from a

to b can be exactly expressed as

$$k_{ab}[\mathscr{S}] = \sqrt{\frac{k_B T}{2m\pi}} Z_a^{-1} \int_{\mathscr{S}_D} e^{-V(\overline{x})/k_B T} d\overline{s}(\overline{x}), \tag{2.1}$$

with k_B being the Boltzmann constant, T the temperature, m the effective mass, $V(\overline{x})$ the potential energy of the system in configuration $\overline{x}$, $Z_a = \int_a e^{-V(\overline{x})/k_B T} d\overline{x}$ the configurational partition function over a, and $\int_{\mathscr{S}_D} d\overline{s}(\overline{x})$ an integral over the dividing surface.

The challenge for TST-based approaches is that one rarely is interested in the transition rate between a and b, but rather the rate that the system transitions between metastable regions of phase space (states) within a and b. We label two metastable regions of phase space within a and b as A and B with $A \subset a$ and $B \subset b$. Since A and B do not necessarily partition phase space, trajectories leaving a through $\mathscr{S}_D$ do not necessarily constitute trajectories traveling from A to B. Thus,

$$k_{AB} \leq k_{ab}[\mathscr{S}_D]. \tag{2.2}$$

While trajectories started in A typically require an unfeasible amount of simulation time before transitioning to B, motivating the TST-based approach, trajectories started on $\mathscr{S}_D$ quickly become members of either A or B. This motivates a combined TST - direct simulation approach as a route to compute k_{AB} [35, 12, 84]. Assuming that trajectories leaving $\mathscr{S}_D$ reach either A or B in a time (t^*) that is short compared to $1/(k_{AB} + k_{BA})$, k_{AB} can be expressed as

$$k_{AB} = \kappa k_{ab}[\mathscr{S}_D], \tag{2.3}$$

where $\kappa = \lim_{N_T \to \infty} \frac{2N_B}{N_T}$ and is often referred to as the transmission coefficient. N_T represents the number of MD simulations started from an equilibrium distribution on $\mathscr{S}_D$ and N_B represents the number of simulations that are in B at

$t = t^*$. For this approach to be effective, $\mathscr{S}_D$ must be chosen such that κ is close to, but less than one. Specifically, if κ is of order much less than one, an unfeasible number of MD trajectories are required to compute κ to reasonable accuracy. As written here, equation 2.3 also assumes that no dynamical bottlenecks exist between A and $\mathscr{S}_D$, i.e. $\kappa < 1$. We note that more general formulations exist where the assumptions of $t^* << 1/(k_{AB} + k_{BA})$ and the absence of dynamical bottlenecks between A and $\mathscr{S}_D$ are not required [84]. Throughout the remainder of this article we will refer to the use of equation 2.3 to compute k_{AB} as ETST. We refer the interested reader to [59, 60, 4] for examples of previous applications of ETST.

A less demanding approach to computing k_{AB} is to assume $\kappa = 1$ and to choose $\mathscr{S}_D = \mathscr{S}_D^{min}$ to reduce the error in this assumption,

$$k_{AB} \approx k_{ab}[\mathscr{S}_D^{min}]. \tag{2.4}$$

This approach is referred to as variational TST (VTST) in the literature [84, 78, 32] and formally consists of choosing $\mathscr{S}_D$ to minimize the total frequency of transitions, $\nu = 2k_{ab}[\mathscr{S}_D]p_a[\mathscr{S}_D]$ with $p_a[\mathscr{S}_D]$ being the probability that the system resides in a relative to b. In practice it is unfeasible to identify $\mathscr{S}_D^{min}$ exactly, thus it is selected from a subset of dividing surfaces. The VTST approach is widely utilized within the chemistry and biophysics communities [75, 7, 57, 49].

Alternatively, one could assume that a potential energy ridge, $\mathscr{S}_D^V$, exists between A and B and that it provides a reasonable approximation to $\mathscr{S}_D^{min}$,

$$k_{AB} \approx k_{ab}[\mathscr{S}_D^V]. \tag{2.5}$$

We will refer to this approximation of k_{AB} as PTST [87].

Due to the computational demands of computing Z_a and the surface integral in equation 2.1, all three of the previously mentioned approaches, i.e. ETST, VTST, and PTST, are often avoided. In fact, to our knowledge none of these methods have ever been applied to the study of dislocation-based mechanisms in the current literature. An eloquent means for avoiding the integrals in equation 2.1 is to assume that the potential energy landscape of the system is locally quadratic (HTST) [87], i.e. a local harmonic approximation. Physically the harmonic approximation equates to assuming temperature independent material properties. Using $\mathscr{S}_D = \mathscr{S}_D^V$, the harmonic approximation in conjunction with the assumption that $\kappa = 1$ gives

$$k_{AB} \approx \left(\frac{\prod_{i=1}^{N} \nu_i^{initial}}{\prod_{i=1}^{N-1} \nu_i^{saddle}} \right) e^{-\frac{\Delta V}{k_B T}}, \tag{2.6}$$

where $\nu_i^{initial}$ represents the i^{th} normal frequency of the system in the configuration of minimum potential energy within a (initial configuration). ν_i^{saddle} represents the i^{th} normal frequency of the system in the configuration of minimum potential energy on $\mathscr{S}_D^V$ (saddle configuration). N represents the number of degrees of freedom in the system, and ΔV is the difference in potential energy between the saddle and initial configurations. The product over the saddle configuration frequencies excludes the imaginary frequency in the direction normal to $\mathscr{S}_D^V$, with all other frequencies being real.

While the computation of equation 2.6 can be less daunting than equation 2.1, the direct calculation of N normal frequencies can quickly become unfeasible for systems where N is large. Two alternative approaches for computing the prefactor in equation 2.6 exist. One entails the direct analytical computation of the ratio of pairs of corresponding normal frequencies away from the defect [81, 52]. The other approach entails the extraction of the prefactor from atomistic simulations constrained to $\mathscr{S}_D^V$ [12, 34].

Many TST-based rate predictions of thermally activated dislocation processes in the literature further simplify the prefactor in equation 2.6 [67, 95, 22, 27]. A straight forward simplification is to assume that it is equal to the frequency in the direction of the reaction coordinate at the initial state

$$k_{AB} \approx \nu_*^{initial} e^{-\frac{\Delta V}{k_B T}}. \tag{2.7}$$

We will refer to this approach as SHTST. It is important to note that since there are multiple meaningful choices of a reaction coordinate to connect the initial and final states, $\nu_*^{initial}$ is not an intrinsic property of the system nor $\mathscr{S}_D$. Alternatively, a continuum estimate [95], the imaginary frequency of the saddle configuration [67], or the Debye frequency are sometimes used as the prefactor.

Often TST rate predictions are presented in terms of an energy barrier [21, 5, 15]. Following Vineyard [87] k_{ab} can be written as

$$k_{ab} = \tilde{\nu} e^{-\Delta F^+ / k_B T}, \tag{2.8}$$

where

$$\tilde{\nu} = \sqrt{\frac{k_B T}{2m\pi}} Z_a^{-1} \int_{\mathscr{S}_0} e^{-V(\bar{x})/k_B T} d\bar{s}(\bar{x}), \tag{2.9}$$

with $\mathscr{S}_0$ being a surface that does not intersect $\mathscr{S}_D$ and contains an initial configuration in a. ΔF^+ is often referred to as the free energy barrier and is written as

$$\Delta F^+ = -k_B T \ln \left(\frac{\int_{\mathscr{S}_D} e^{-V(\bar{x})/k_B T} d\bar{s}(\bar{x})}{\int_{\mathscr{S}_0} e^{-V(\bar{x})/k_B T} d\bar{s}(\bar{x})} \right). \tag{2.10}$$

Physically ΔF^+ can be thought of as the potential of mean force required to move the system from $\mathscr{S}_0$ to $\mathscr{S}_D$. Further insight can be gained by decomposing ΔF^+ into an internal energy barrier, ΔU^+, and entropic energy barrier, ΔS^+, i.e. $\Delta F^+ = \Delta U^+ - T\Delta S^+$. Under the harmonic approximation $\Delta U^+ = \Delta V$, but in

general ΔU^+ is a function of the expected values of potential energy on $\mathscr{S}_D$ and $\mathscr{S}_0$, $\Delta U^+ = \langle V(\bar{x})\rangle_{\mathscr{S}_D} - \langle V(\bar{x})\rangle_{\mathscr{S}_0}$. It is important to emphasize that $\tilde{\nu}$, ΔF^+, ΔU^+, and ΔS^+ are not intrinsic physical properties with respect to $\mathscr{S}_D$ as they are dependent upon $\mathscr{S}_0$. However, often in practice, and consistent with our findings here, $\tilde{\nu}$, ΔF^+, ΔU^+, and ΔS^+ are not appreciably dependent upon the choice of $\mathscr{S}_0$ so long as it is physically reasonable, e.g. normal to the minimum potential energy or maximum probability reaction paths and containing a minimum energy state in a.

It is instructive to note the behavior of the various TST-based approaches in the limit of $T \to 0$. In this limit, the harmonic approximation becomes exact and the local potential energy along the reaction coordinate dominates the process. Thus, $\mathscr{S}_D^{min} \to \mathscr{S}_D^V$ and VTST, PTST, and HTST predictions coincide. The relative error between the SHTST and HTST predictions will remain constant irrespective of temperature. The ETST prediction will not necessarily coincide with VTST, PTST, and HTST as $T \to 0$ for arbitrary potential energy landscapes.

2.4 Numerical Methods

The atomistic simulations were conducted using a modified version of the freely available LAMMPS package [58]. Atomic interactions were modeled using an Al Embedded Atom Potential developed by Mishin et al. [50] that has been shown to predict athermal dislocation nucleation loads in reasonable agreement with Density Functional Theory calculations [54]. All simulations consisted of fully periodic simulation cells filled with an fcc Al lattice. The lattice constant and unloaded cell dimensions corresponded to a zero pressure equilibrium state

with $a_0^{0K} = 4.050$and $a_0^{300K} = 4.065$. Geometric features, i.e. cylindrical void or pyramidal free surface, were created by the removal of atoms. The simulation cells investigated here, and shown in figures 1 and 3, were composed of 1,080 and 191,000 atoms, respectively. Shear loading was applied by adjusting the simulation cell shape. The stress was computed using the Virial Theorem.

NVT Molecular dynamics simulations were performed in a variety of contexts in this work. In all cases the simulations were conducted at 300K using a Langevin thermostat with a damping parameter of 1ps [69]. A time step of 1fs was used within a velocity Verlet integration scheme.

For the TST-based calculations, phase space was sampled within fixed simulation cells using a parallel implementation of the most recent version of the Finite Temperature String (FTS) Method by Vanden-Eijnden and Venturoli [85]. Steps of the algorithm is described in detailed in appendix A. The method consists of dividing configuration space into a set of Voronoi cells, whose centers represent a series of intermediate configurations (images) between a given initial and final configuration. The curve connecting the images in configuration space defines the string.

Atomistic simulations sampling configuration space with a finite temperature Boltzmann distribution are then started from each image and allowed to evolve under the constraint that they remain inside the Voronoi cell in which they were started. The average positions of these simulations in configuration space are then used to define a new string with new Voronoi cell centers equally spaced. Iterating over this process leads to a converged string that represents a temperature dependent principle curve between the initial and final states.

The probability of the system configuration to exist within a specific cell can then be obtained by performing further Boltzmann sampling in each cell of the converged string. By computing the probability, h_{ij} that a configuration within a cell i will attempt to move to cell j during the next time step, the probability, f_m, that the configuration of an equilibrated system resides in the cell m, relative to all other cells can be obtained by solving

$$\sum_{i=0}^{n} f_i h_{ij} = \sum_{i=0}^{n} f_j h_{ji}, \sum_{i=0}^{n} f_i = 1, \tag{2.11}$$

with n being the number of cells.

Limiting the selection of dividing surfaces to the set of hyperplanes perpendicular to the string, the ratio of configuration space integrals in equation 2.1 can be approximated as

$$Z_a^{-1} \int_{\mathscr{S}_D} e^{-V(\bar{x})/k_B T} d\bar{s}(\bar{x}) \approx \frac{f_i}{\sum_{j=0}^{j=i} f_j w_i}, \tag{2.12}$$

where i represents the cell which straddles the dividing surface and w_i is the spacing between the cell walls of i along the string.

In our application to dislocation nucleation, the initial and final configurations (images) from which the starting string is constructed were obtained from direct MD simulation at a high load where nucleation occurs quickly. The configurations captured from MD were scaled to the desired shear strain for the specific string calculation. The starting intermediate images were created by linear interpolation. The simulations conducted in this work used between 30 and 100 images with a typical spacing of ~ 0.5. The string algorithm was modified so that the position of the initial image and the string length remained fixed during the simulation. This enabled a nonequilibrium final image to be used, which considerably reduced the computational expense. The atomistic simu-

lations used to compute both the string path and h_{ij} over the converged string were conducted in the overdamped limit [85].

For the HTST and SHTST predictions, the potential energy barrier of the reaction is required. We have computed the potential energy barrier using the string method in the limit of $T \to 0$ using a simulation cell with dimensions corresponding to the 0K equilibrium lattice constant. Subsequently, the string computed at 0K (which we subsequently refer to as the 0K string) follows a different path in configuration space than the string computed at 300K. To investigate the difference between these two strings and the accuracy of key approximations in common TST-based approaches, we compute the values of ΔF^+, ΔU^+, and ΔS^+ at 300K along each string. For the HTST and SHTST predictions, the normal modes of the minimum energy and saddle configurations were computed by finding the eigenvalues of the stiffness matrix.

2.5 Comparison of TST-based Approaches

The utility of the each of the five TST-based approaches described in section 2 was tested by examining the mean or expectation time ($\bar{t} = k_{AB}^{-1}$) for dislocation nucleation from the surface of a cylindrical nanovoid (d=1.2nm) in a small periodic simulation cell loaded in shear (figure 2.1). To avoid the complexities associated with competing nucleation events on different planes, a small irregularity was created on the surface of the void by removing a few atoms. The critical shear load at which dislocation nucleation occurs instantaneously was identified from direct MD simulation at 300K as 1.4GPa for this specimen. A benchmark for assessing the TST-based predictions was then created by performing

100 nominally identical but statistically different MD simulations within a fixed simulation cell corresponding to a shear load of 1.1GPa and zero normal loads at 300K. The expectation time for dislocation nucleation in this set of simulations was found to be 17ns. Assuming a Poisson process, the true expectation time for dislocation nucleation is then between 14 and 21ns using a 95% confidence interval.

As expected, the ETST prediction best corresponds to the direct MD simulations, $\bar{t}^{ETST} = 1/k_{AB}^{ETST} = 14ns$. The hyperplane perpendicular to the 300K principle curve that minimized $Z_a^{-1} \int_{\mathscr{S}_D} e^{-V(\bar{x})/k_B T} d\bar{s}(\bar{x})$ was used as the dividing surface, i.e. $\mathscr{S}_D \approx \mathscr{S}_D^{min}$. 100 direct MD simulations were performed from the dividing surface to compute the transmission coefficient, $\kappa = 0.90$, following [84]. The difference between the ETST and MD predictions highlights that the string method only provides an approximate dividing surface between states as indicated in equation 2.12. While refinement of the string cell spacing (w) can improve the finite width approximation, the hyperplane approximation of the dividing surface ultimately limits accuracy in cases where the string is curved in configuration space, such as in this work. With κ near unity and $\mathscr{S}_D \approx \mathscr{S}_D^{min}$, the VTST rate approximation is similar to the ETST result (table 1). The consistency between the VTST and ETST predictions is indicative of a well chosen dividing surface and a process governed by a well defined energy barrier between metastable states.

To provide insight into the nucleation processes and set a foundation for better understanding the PTST, HTST, and SHTST approaches, we provide the energetic details of the Voronoi cells whose centers define the 300K principle curve (string) associated with the nucleation process (figure 2.2(a)). All the

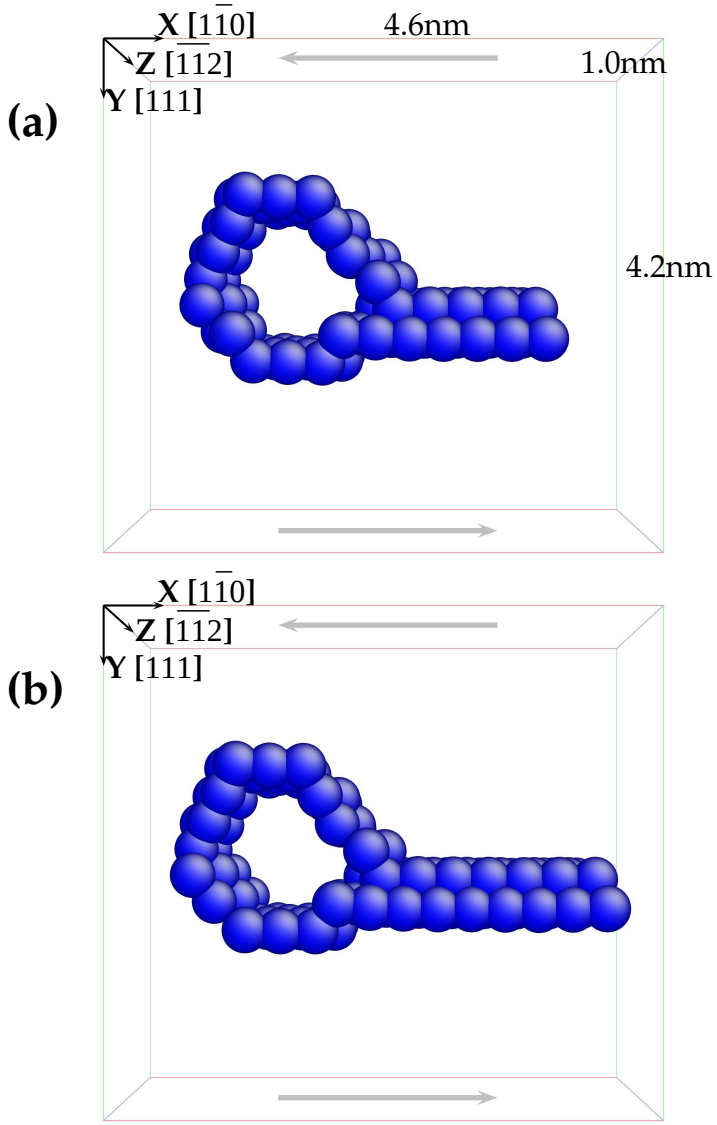

Figure 2.1: Image of cylindrical nanovoid simulation geometry used to study dislocation nucleation in Al at 300K. (a) depicts the cell center configuration corresponding to the VTST dividing surface along the 300K string, i.e. $\mathscr{S}_D^{min}$. (b) depicts the cell center corresponding to the potential energy barrier along the 0K string, i.e. $\mathscr{S}_D^V$. In both cases the configurations do not involve trailing partial dislocations. The atoms in perfect fcc stacking are not shown [41]. Accordingly, the atoms shown depict the surface of the nanovoid and the stacking fault associated with the nucleating partial dislocation.

Method	$\bar{t}(ns)$	$\Delta F^{+}(eV)$	$\Delta U^{+}(eV)$	$\Delta V^{+}(eV)$	$T\Delta S^{+}(eV)$	CPU hours
Direct MD	17	-	-	-	-	1000
ETST	14	0.245	0.453	0.420	0.208	130
VTST	13	0.245	0.453	0.420	0.208	120
PTST	1.3	0.147	0.438	0.670	0.291	70
HTST	640	0.330	0.670	0.670	0.340	30
SHTST	310×10^6	0.670	0.670	0.670	0.000	27

Table 2.1: Expectation time predictions and energetics associated with dislocation nucleation from an Al cylindrical nanovoid at 300K using five TST-based approaches. The last column gives the approximate computational expense associated with each approach for the 3,240 degree of freedom simulation cell on an X5355 Intel Xeon 2.7GHz processor.

measured energies are referenced with respect to the first cell of the string, $i = 0$, corresponding to an un-nucleated configuration. The free energy of cell i relative to cell $i = 0$ is given as $F_i = -k_B T \ln(f_i/f_0)$, the internal energy as $U_i = \langle V(\bar{x})\rangle_i - \langle V(\bar{x})\rangle_0$, the entropy as $S_i = (U_i - F_i)/T$, and the potential energy as $V_i = V(\bar{x_i}) - V(\bar{x_0})$. $\langle V(\bar{x})\rangle_i$ represents the ensemble average of the potential energy in cell i and x_i represents the minimum potential energy configuration in cell i near the string. As $T \to 0$, $U_i \to V_i$. Connecting with the activation energy barriers defined in section 2, one can approximate $\Delta F^{+} \approx F_j$ with j representing the cell that straddles the corresponding dividing surface.

Three characteristics of energy curves deserve comment. First, U_i and V_i are not equivalent as assumed with a harmonic approximation, yet they do exhibit maximums at nearly the same location along the string. Second, F_i exhibits a maximum significantly earlier than V_i and U_i indicating that $\mathscr{S}_D^V \neq \mathscr{S}_D^{min}$. Third, S_i is of significant magnitude and it increases with distance along the string, consistent with the second comment.

In general, the significant change in entropy during the nucleation process

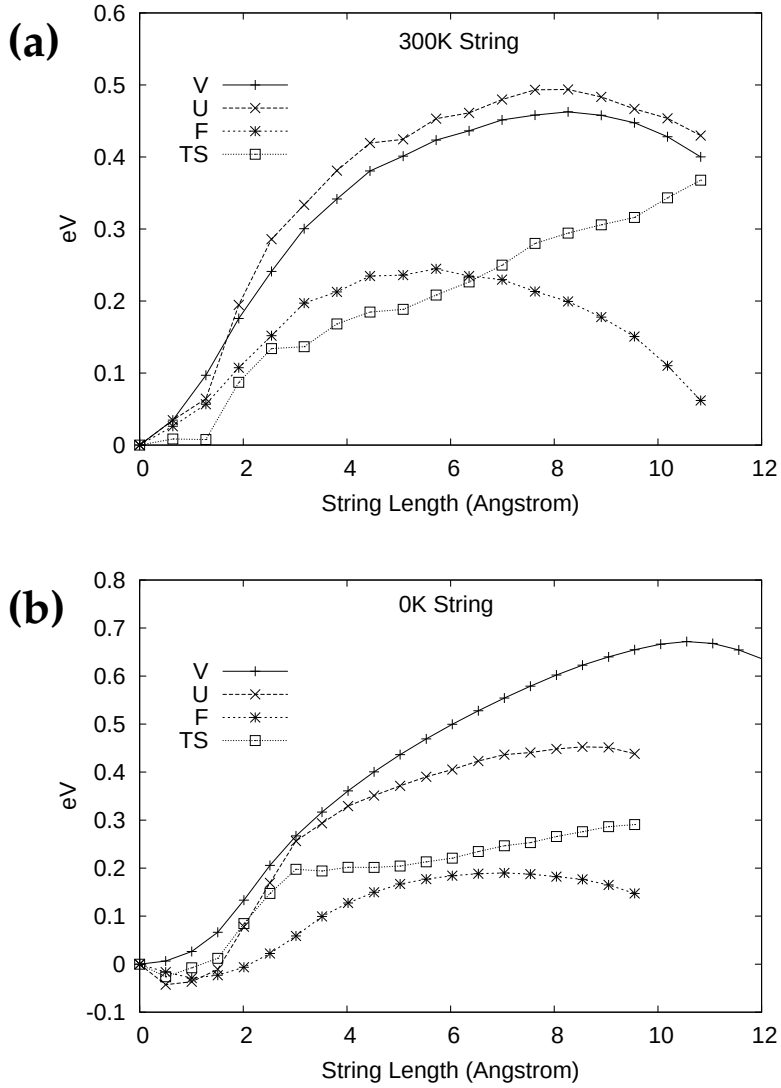

Figure 2.2: Cell energies along the 300K (a) and 0K string (b) corresponding to the dislocation nucleation process associated with the simulation setup shown in figure 2.1. U, F, and TS were obtained by 300K sampling along the respective strings.

(figure 2.2(a)) is consistent with other studies of dislocation nucleation [25] and the nucleation of other solid state defects [81]. The role of entropy can be understood by considering that, to leading order, entropy is a measure of how strongly the free energy of the system depends on temperature. Since the free energy of the partial dislocation and the associated stacking fault are linked to the elastic constants and stacking fault energies of the crystal, which are temperature dependent [89], it follows that the temperature dependence of the systems free energy increases as the dislocation forms and the stacking fault area grows. Thus, the entropy should be expected to increase as the dislocation nucleates. At later stages in the nucleation processes successive configurations primarily differ by the position of the partial dislocation and thus the total area of stacking fault. This is consistent with the nearly linear increase in entropy observed during the later stages of nucleation (figure 2.2(a)). Finally we note that this explanation is consistent with previous studies of thermally activated dislocation processes that consist of a dislocation in both the initial and saddle states where entropy was found to play a much less significant role [34, 86].

The PTST, HTST, and SHTST approaches are explicitly based on the potential energy landscape of the system. Thus, we have also computed the minimum energy path, i.e. a 0K principle curve (string), connecting the minimum potential energy un-nucleated configuration with a nucleated configuration. The configuration of maximum potential energy along this curve represents the potential energy saddle configuration and the hyperplane perpendicular to the principle curve at this point locally approximates $\mathscr{S}_D^V$. The potential energy analysis cannot be conducted at both the same volume/strain and pressure/load as the direct MD analysis due to the temperature dependent properties of the system. Furthermore, whether volume/strain or pressure/load are chosen to

correspond to the direct MD analysis can significantly influence the resulting rate prediction. Performing the 0K analysis at the same cell volume/strain as a 300K MD analysis is not straight forward as geometric stress risers and material heterogeneities can lead to the disappearance of the potential energy dividing surface. Accordingly, here we perform the 0K potential energy analysis in a fixed simulation cell corresponding to an initial configuration of zero hydrostatic pressure and 1.1GPa shear stress, consistent with the 300K MD simulations.

The energetics of the 0K string are given in figure 2.2(b). The most significant difference relative to the 300K string is that the potential energy of the cell centers increases to a much higher maximum. Thus the potential energy barrier for dislocation nucleation is significantly greater at 0K relative to 300K for the same stress field. Our computation of F_i, U_i, and S_i with 300K sampling along the 0K string yielded only meaningful values at cells with centers less than 10 from the initial image of the string. Specifically, for cells associated with distances greater than 10 along the string, the Markov sampling within the cell transitioned outside of the local reaction tube to configurations of significantly lower energy [85]. Accordingly the values of F_i, U_i, and S_i associated with cells having centers greater than 10 are not indicative of the nucleation process and are not displayed in figure 2.2(b). Nonetheless, insight can still be drawn from the values of F_i, U_i, and S_i that are available. First, F_i and U_i decrease below zero energy during the initial stages of nucleation. This indicates that the initial string image which was fixed at the minimum potential energy configuration in the un-nucleated state is different from the average configuration (minimum free energy configuration) in the un-nucleated state, consistent with thermal expansion from the anharmonicity of the system. Second, the difference between

the maxima of U_i and V_i is much greater for the 0K string compared to the 300K string, something which will lead to significant error when using the harmonic approximation. Third, the maxima of F_i and U_i associated with the nucleation process are similar between the 300K and 0K strings. These later two points combined with the differences in V_i between the 0K and 300K strings are telling of the performance of the PTST, HTST, and SHTST approaches.

Considering that $\mathscr{S}_D^V$ intersects the string at 10.5, an approximate PTST prediction can be computed using the cell centered around 9.5 to estimate the PTST dividing surface statistics (figure 2.2(b)). Using this approach, the PTST prediction is consistent with the theory developed in section 2 in that it over predicts the rate relative to the VTST result (table 1). This result can be mostly attributed to the difference in position between $\mathscr{S}_D^V$ and $\mathscr{S}_D^{min}$. Physically the difference in the dividing surfaces equates to different leading partial dislocation saddle state positions (figure 2.1). This can be largely attributed to the temperature dependence of stacking fault energies and elastic constants, as these properties influence the forces experienced by the dislocation [89] which determine its saddle state configuration. Thus, while PTST incorporates temperature dependent phenomenon, its reliance on $\mathscr{S}_D^V$, a temperature independent quantity leads to increased error relative to VTST. Congruously, we note that if VTST is performed using the 0K principle curve, an expectation time of 6ns is predicted.

The HTST approach explicitly utilizes an assumption of material property temperature independence, i.e. a harmonic approximation. The error associated with this approximation leads to a severe under prediction of the nucleation rate (table 1). Energetically, errors in both U_i and S_i act in opposition to each other. However the error in U_i dominates as it is almost 40% greater than cor-

responding PTST value, thus resulting in an underprediction of the nucleation rate. Accordingly, we find the most significant error of the HTST approach to be due to the approximation $U_i = V_i$, which is consistent with the anharmonicity of the system.

The SHTST approach assumes a zero entropy barrier. Therefore, its predictive ability is very poor, with an expectation time prediction seven orders of magnitude too large. Thus, the precise choice of the SHTST prefactor is irrelevant, e.g. the imaginary frequency of the saddle state ($0.62ps^{-1}$), a continuum estimate of a fluctuating dislocation line ($0.60ps^{-1}$) [63], the value from equation 2.9 with $\mathscr{S}_0$ being the first hyperplane of the string ($0.62ps^{-1}$), or even the Debye frequency ($12ps^{-1}$).

Overall, we find that the accuracy of TST-based approaches for predicting dislocation nucleation rates generally scales with computational expense when using the string method (table 1). If it is necessary to avoid the algorithmic complexity and large number of interatomic force calculations associated with sampling configuration space, as with PTST, VTST, and ETST approaches, then the harmonic approximation must be utilized. An example of such situation would be an application that requires accurate interatomic forces to be computed using a method such as density functional theory. In this case sufficient sampling of configuration space is currently unfeasible for all but the smallest systems, motivating the use of the harmonic approximation. However, the error associated with the standard HTST approach, as proposed by Vineyard [87] and utilized here, is particularly problematic in that it can also lead to the incorrect prediction of relative rates between deformation mechanisms. An relevant example is the competition between vacancy diffusion and dislocation nucleation in a

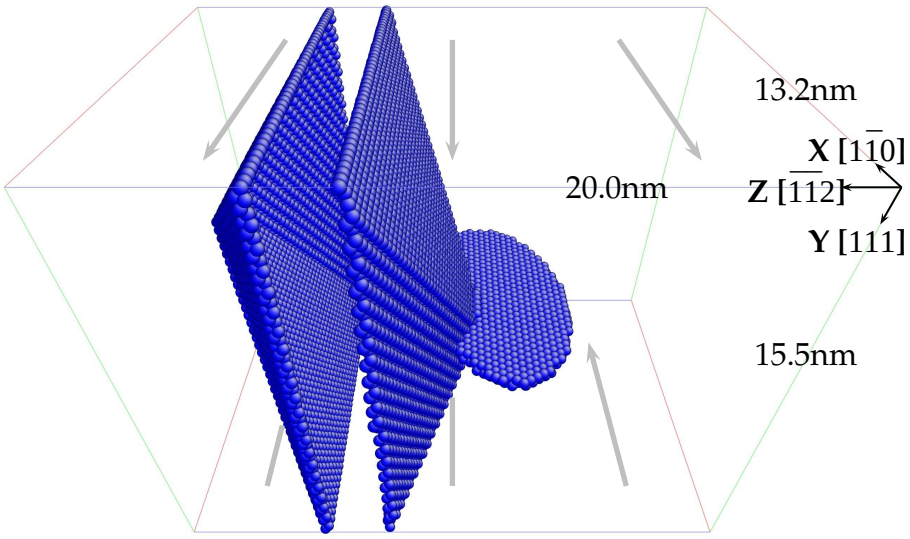

Figure 2.3: Image of simulation geometry used to study dislocation nucleation from a faceted surface in Al at 300K. The atoms in perfect fcc stacking are not shown [41]. Accordingly, the atoms shown depict the pair of Al surfaces in the periodic simulation cell and the stacking fault associated with a nucleating partial dislocation loop.

stressed material. In this case, HTST would likely be much more accurate for the latter and thus skew the relative rates. Perhaps the most effective approach for mitigating the errors associated with HTST would be to apply the harmonic approximation about the finite temperature state (i.e. use a quasi-harmonic approximation). Beyond this, further improvement could be obtained by using quasi-HTST in a variational context along the reaction coordinate such that the rate prediction is minimized (as done here with VTST).

2.6 Application: Dislocation Nucleation from a Surface

As an initial application of our findings, we have investigated dislocation nucleation from a surface. While this topic has been continually studied for over 50 years [20] a renewed excitement currently surrounds it due to expanding interest in nano-dimensioned materials. Specifically, in many crystalline materials a decrease in specimen dimensions or internal microstructural dimensions to submicron length-scales brings about a significant increase in strength [14, 39, 66]. This strengthening trend, due to the length-scale effects associated with traditional deformation mechanisms, is then limited by the stress at which other nontraditional deformation mechanisms begin to be activated. Thus, the stress required for dislocation nucleation from a surface represents an upper bound for strength of many materials.

Here we have investigated dislocation nucleation from a faceted Al surface at 300K loaded in shear (figure 2.3). As with the cylindrical nanovoid studied in section 4, care was taken to construct an irregular geometry that favored dislocation nucleation from a specific site on a single plane, i.e. the intersection point of 4 facets. We note that due to the periodicity of the simulation cell, two surfaces exist. One was made more favorable for nucleation by removing a few atoms near the intersection point of the facets. While this atomic-scale defect made a particular surface more favorable to nucleation than the other, it did not have a noticeable effect on the load at which instantaneous nucleation occurred (to within 5%).

We performed two VTST and several direct MD simulations. Strain controlled direct MD simulations were used to identify the critical load at which

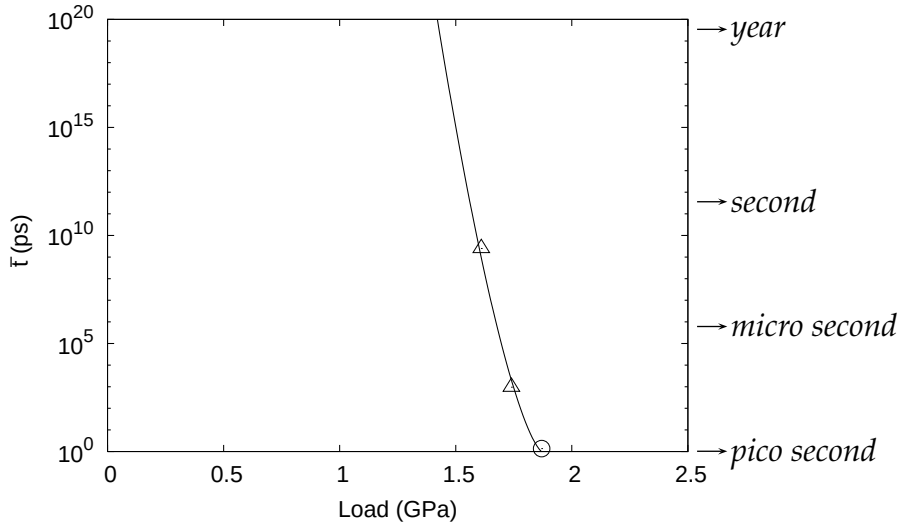

Figure 2.4: The expectation time for dislocation nucleation from a faceted surface versus applied shear stress in Al at 300K. The picosecond data point was computed using direct MD while the points corresponding to longer times were computed using variational TST. The model curve was generated by fitting the atomistic simulation data points to equation 2.13.

dislocation nucleation occurs instantaneously (less than a few picoseconds), $\tau = 1.9GPa$. The VTST calculations were then used to compute the expectation time at two subcritical loads. The discrete simulation data points were then interpreted with regard to a continuous range of loadings using equation 2.8 and a standard expression for the energy barrier [38],

$$\Delta F^{+} = \Delta F_0^{+} \left(1 - \frac{\tau}{\tau_0}\right)^{3/2}, \tag{2.13}$$

where $\tilde{\nu} = 0.62ps^{-1}$, τ is the applied shear stress, and τ_0 the critical applied stress. $\Delta F_0^{+} = 1.9$eV was identified as the best fit to the data. The most striking feature of our predictions is the rate at which $\bar{t}$ increases with decreasing load (figure 2.4). Thus, at loads below 80% of the critical load dislocation nucleation would not be expected to occur at a rate sufficient to contribute to material deformation at typical experimental time scales.

To provide context for these values, we note recent measurements of the tensile strength of Al nanowires by Legros et al. [40]. The authors report tensile strengths of 1GPa for 200nm diameter Al wires. Considering that our simulations were conducted under pure shear loading, the experimental strengths are significantly below the stresses at which we predict dislocation nucleation to occur. Nonetheless, there are significant differences between our predictions and the experiments that need to be noted, e.g. surface geometry [94], normal stresses acting on the nucleation plane [8], and surface oxide effects.

An additional connection to mechanical testing can be drawn from the dependence of $\bar{t}$ on load. In a material where plastic flow is controlled by dislocation nucleation, the plastic strain rate, $\dot{\gamma}$, can be considered proportional to $1/\bar{t}$ which is a function of applied load, τ. Accordingly, our VTST modeling predictions combined with equation 2.13 forecast the strain rate sensitivity of Al deformed at 300K to be $m = \partial ln\tau / \partial ln\dot{\gamma} = 0.005$ if deformation is controlled by dislocation nucleation. We note this value is not very sensitive to specimen geometry for a given nucleation rate, based on our own preliminary studies that we will publish separately. However, m is dependent upon nucleation rate, with $m = 0.005$ corresponding to millisecond nucleation rates while $m = 0.007$ corresponds to nanosecond nucleation rates. This emphasizes the fact that strain rate sensitivities measured from direct MD simulations will typically be larger than those associated with the same deformation mechanism at experimental timescales.

Experimentally the rate sensitivity of Al at room temperature has been measured for both coarse grained, $m \approx 0.004$ [48], and nanocrystalline forms, $m \approx 0.08$, [19]. Interestingly, our predictions correspond more closely with

coarse grained Al, where dislocation nucleation is known to not be a controlling process, as opposed to nanocrystalline Al where dislocation nucleation has been considered as a candidate deformation mechanism [39, 19, 42]. Thus, we reach two conclusions. First, the strain rate sensitivity signature of dislocation nucleation is not significantly different than that of coarse grained deformation mechanisms. Second, it is unlikely that dislocation nucleation is a controlling deformation mechanism in nanocrystalline metals, a conclusion that is consistent with other recent work in this area [8].

2.7 Conclusions

This work has examined the utility of five TST-based approaches for predicting dislocation nucleation. Using a parallel implementation of the finite temperature string method and focusing on Al at 300K, we have demonstrated that two TST-based approaches can accurately predict nucleation rates. The multi-method investigation and complete energetic analysis of the nucleation process illuminated key sources of error in more approximate and commonly used TST-based approaches, e.g. a large entropy barrier associated with the nucleation process. Thus, this work provides guidance for future TST-based studies of dislocation processes and motivates further investigation into the utility of other TST-based approaches not considered here.

As an initial application of these findings, we have performed a variational TST study of dislocation nucleation from a free surface in Al under ordinary laboratory conditions. The predicted nucleation stresses are significantly above the highest strengths that have been observed for pure Al, indicating the possibility

of even higher experimental strength observations in the future. Furthermore, the predictions provide a strain rate sensitivity signature that can be associated with dislocation nucleation controlled deformation. While the rate sensitivity associated with dislocation nucleation does not differ from the value associated with traditional dislocation processes occurring in coarse grained Al, it does differ from values associated with nanocrystalline Al. This suggests that while dislocation nucleation may occur at internal stress concentrations and grain boundaries in nanocrystalline Al, it is not the rate limiting process.

2.8 Acknowledgments

The authors acknowledge support from Paul Hess at ONR (Grant N00014-08-1-0862 and N00014-10-1-0323 and Ed Glaessgen and Steve Smith at NASA (Grant NNX08BA39A).

CHAPTER 3

THE IMPROBABILITY OF VOID GROWTH IN ALUMINUM VIA DISLOCATION NUCLEATION UNDER TYPICAL LABORATORY CONDITIONS

By Linh D. Nguyen and Derek H. Warner

As published in *Physical Review Letters* **108** (2012) 035501

3.1 Abstract

The rate at which dislocations nucleate from spherical voids subjected to shear loading is predicted from atomistic simulation. By employing the latest version of the Finite Temperature String Method, a Variational Transition State Theory approach can be utilized, enabling atomistic predictions at ordinary laboratory timescales, loads, and temperatures. The simulation results, in conjunction with a continuum model, show that the deformation and growth of voids in Al is not likely to occur via dislocation nucleation under typical loadings regardless of void size.

3.2 Introduction

The failure of many modern engineering alloys is controlled by the growth and coalescence of internal voids. At high temperatures void growth is thought to occur via diffusion, while at lower temperatures, shorter times, and/or higher loads, void growth is often attributed to dislocation plasticity. The plastic

growth of large voids (10s of microns) is scale independent and can accurately be described by traditional continuum plasticity theory, with the void size being sufficiently larger than the length-scales of dislocation plasticity. Popular engineering fracture models are formulated upon this foundation [24, 65]. The plastic growth of smaller voids is dependent upon their size, with the length-scale of the stress/strain perturbation created by the void being on the order of the mobile dislocation and dislocation source spacing. Accordingly, the plastic growth of smaller voids must be described using scale dependent plasticity theories [17, 11] (or discrete dislocation simulations [33, 70]) to capture the smaller→stronger trend observed in experiment [76, 2]. The smallest voids, having nanometer dimensions, produce stress perturbations that interact with at most a few mobile dislocations and dislocation sources. Consequently, the growth of nanovoids is thought to depend upon the nucleation of dislocations from their surface. A large literature investigating this process has developed in the past decade.

Continuum analyses of dislocation nucleation from voids have been conducted by several independent research groups, e.g. [2, 1, 79, 80, 16, 44, 88]. The athermal analyses unanimously suggest that dislocation nucleation from the surface of a void is viable under very high loads. However, the qualitative insight offered by such analyses is limited in that significant geometric and parametric assumptions are often employed to make the analyses analytically tractable. Considering the nanoscale dimensions of the problem, atomistic simulations can provide a powerful investigative tool. In accordance with the continuum analyses, the simulations suggest that dislocation nucleation from voids is possible at very high loads and short timescales [79, 71, 72, 46, 47, 61, 77, 93, 9]. This is consistent with post-testing microscopy in laser shocked Cu (~5GPa for

~10ns) [45]. However, the plausibility of dislocation nucleation from voids under ordinary laboratory loads and longer time scales, where thermal activation can play a significant role, remains unclear. Here, we explore this question using a newly developed atomistic simulation technique that enables the accurate calculation of finite temperature nucleation rates at timescales well beyond those accessible to standard molecular dynamics (MD) simulations.

3.3 Approach and Simulation Setups

In this work, dislocation nucleation under ordinary experimental conditions is investigated with atomistic resolution in a Variational Transition State Theory (V-TST) framework using the latest version of the Finite Temperature String (FTS) Method [85]. Both the V-TST approach and the Al interatomic potential [50] used here have recently been shown to accurately predict dislocation nucleation relative to direct MD and electronic structure simulations [56, 54]. Nucleation from several nanovoid sizes and a free surface is examined at several loads. The results are then used as fitting data for a continuum model to provide predictions of dislocation nucleation rates across a range of meaningful void sizes and loads.

The V-TST framework provides a means to predict the rate at which a thermally activated event, such as dislocation nucleation, will occur [56, 84, 32],

$$k = \sqrt{\frac{k_B T}{2m\pi}} Z_a^{-1} \int_{\mathscr{S}_D} e^{-V(\bar{x})/k_B T} d\bar{s}(\bar{x}), \tag{3.1}$$

with k_B being the Boltzmann constant, T the temperature, m the effective mass, $V(\bar{x})$ the potential energy of the system in configuration $\bar{x}$, and $Z_a = \int_a e^{-V(\bar{x})/k_B T} d\bar{x}$ the configurational partition function over a. $\int_{\mathscr{S}_D} d\bar{s}(\bar{x})$ represents an integral

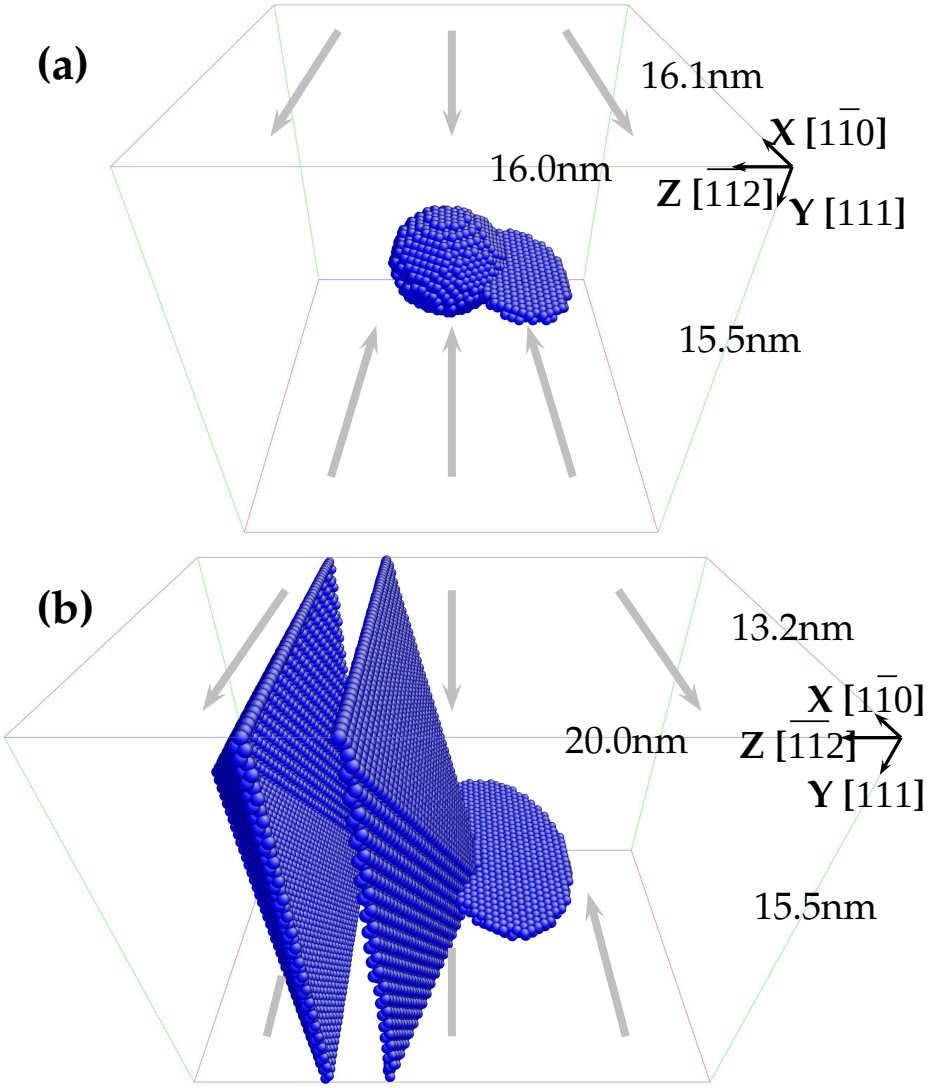

Figure 3.1: Images of simulation cell geometries and loadings. (a) and (b) represent the D = 4nm spherical void and faceted surface specimens at applied loads of 1.7GPa and 1.6GPa, respectively. In both cases the configurations represent the activated states, which only involve leading partial dislocations. The atoms in perfect fcc stacking are not shown [41]. Accordingly, the atoms shown in (a) depict the surface of the void and the stacking fault associated with the nucleating partial dislocation loop, and in (b) depict the pair of Al surfaces and the stacking fault associated with the nucleating partial dislocation loop [41].

over a surface in configuration space, which in this case separates the set of unnucleated configurations from nucleated configurations. The term "variational" denotes the fact that $\mathscr{S}_D$ is chosen to minimize the total frequency of transitions between the unnucleated and nucleated states, $\nu_{tot}^{freq} = 2kp_{un}$ with p_{un} being the probability that the system exists in an unnucleated configuration.

The primary challenge in obtaining a V-TST rate prediction is the computation of the integrals in equation 3.1. For this we use a parallel implementation of the FTS method [85]. The method is built upon a set of points in configuration space, which define a curve connecting an unnucleated and nucleated configuration. Voronoi cells are defined about each point in configuration space and the configuration space within each cell is sampled via independent simulations at 300K. The cell centers are iteratively adjusted until they represent the average configuration associated with the sampling within each cell subject to an equal cell center spacing constraint. After the position of the cell centers converge, the relative probability for the system to exist in each cell can be obtained by tabulating the frequency at which the simulations attempt to sample configurations in neighboring cells. Limiting the selection of the dividing surface, $\mathscr{S}_D$, to the set of hyperplanes perpendicular to the string, the ratio of configuration space integrals in equation 3.1 can then be approximated as

$$Z_a^{-1} \int_{\mathscr{S}_D} e^{-V(\overline{x})/k_B T} d\overline{s}(\overline{x}) \approx \frac{f_i}{\sum_{j=0}^{j=i} f_j w_i}, \tag{3.2}$$

where i represents the cell that straddles a particular choice of $\mathscr{S}_D$, w_i the spacing between the cell walls of i along the string, and f_i the probability that the system is in cell i. The sampling of the atomistic configuration space was performed in the overdamped limit [85] using a modified version of the LAMMPS package [58] and an Al Embedded Atom Potential [50]. Between 30 and 100 cells were used in the calculations with a typical cell width of $\sim$ 0.5. The overall string

length was held fixed enabling a nonequilibrium nucleated configuration to be used for the end cell.

Three nanovoids of diameters D = 4nm, D = 6nm, D = 8nm and a faceted Al surface were examined. The specimens were strained in shear by adjusting the shape of the fully periodic cell (figure 3.1). The fcc lattice constant and unloaded cell dimensions corresponded to a zero pressure equilibrium state with a_0^{300K} = 4.065. The crystallography and loading direction were chosen to provide the limiting case, i.e. most favorable for nucleation. The cells were composed of between 191,000 and 325,000 atoms such that the distance between free surfaces remained constant. To break the symmetry of the cell and provide a single preferred nucleation site a few surface atoms were removed at one of the two peak shear stress locations. This did not have a significant (< 7%) effect on the critical shear load at which instantaneous (less than a few picoseconds) nucleation occurred. The influence of the facets in the free surface simulation was examined at 0K, where the athermal nucleation stress was found to be 3% lower than the critical stress in an analogous simulation with no facets, i.e. a flat [112] surface.

Standard NVT MD simulations were performed to determine the critical loads and to acquire the configurations needed to initialize the string. The simulations were conducted with a 1fs time step at 300K using a Langevin thermostat with a damping parameter of 1ps [69]. The critical shear loads were found to be 2.16GPa, 1.89GPa, 1.70GPa and 1.90GPa for the voids of diameter D = 4nm, D = 6nm, D = 8nm and the faceted surface, respectively. Nucleation from the faceted surface can be interpreted as nucleation from a spherical void with $D \to \infty$ by dividing the applied loading, τ, by the shear stress concentration factor of 1.87 [26], giving τ_{crit} = 1.02GPa for $D \to \infty$. The smaller→stronger

size effect observed here can be understood by considering that the finite size of the emerging dislocation core is acted upon by a force ($stress \times area$) that is dependent upon the size of the void [1, 44, 88].

3.4 Results and Discussion

In figure 3.2(a) the direct MD critical load predictions are given with the V-TST predictions at subcritical loads for two void sizes and the faceted surface. The nucleation rate is found to quickly go to zero as the load is decreased from the critical load. The strong dependence on load is indicative of the process having a relatively large activation volume, and is in accordance with the expected dividing surface configurations (activated state) shown in figure 3.1. The presence of a significantly sized dislocation loop and stacking fault area in the activated state (but not in the initial state) is the key feature that necessitates the use of advanced TST approaches, e.g. V-TST, as opposed to more approximate TST approaches, e.g. Harmonic TST. Specifically, the presence of a large temperature dependent defect only in the activated state can create a significant difference between the free energy and potential energy profiles along the reaction coordinate (figure 3.3). Differences in both the energy barrier height and position become more significant with decreasing load, as the dislocation loop in the activated state becomes larger. This finding is consistent with two recently published works that have highlighted the importance of considering the free energy profile when predicting dislocation nucleation [56, 68].

To obtain predictions of dislocation nucleation rates across a range of meaningful void sizes and applied loads, the simulation data points were interpo-

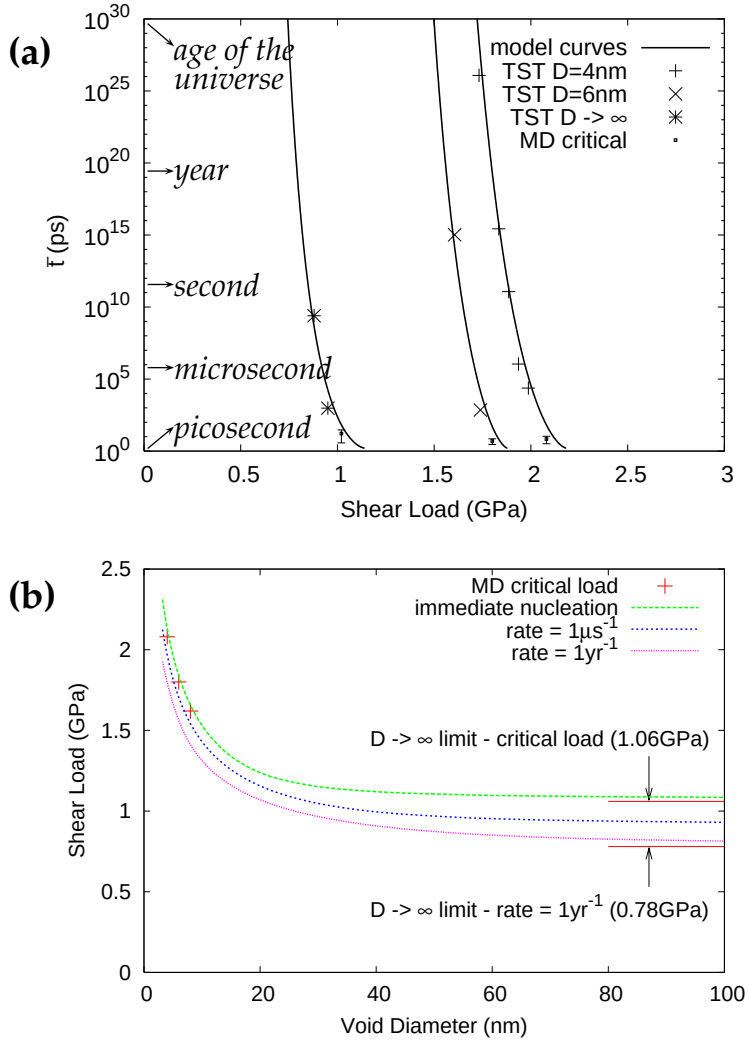

Figure 3.2: (a) The expectation time for dislocation nucleation from a spherical void versus applied shear stress. The picoseconds data points were computed using direct MD while the points corresponding to longer times were computed using V-TST. The vertical bars on the MD data points correspond to the standard deviation of nucleation times collected from 50 independent simulations. (b) The applied shear stress required to achieve the specified nucleation rate as a function of spherical void size.

lated/extrapolated using an isotropic elastic continuum model that provided physical guidance. For our purpose, the specific details of the model have little consequence on the final conclusions. The model was constructed from an Arrhenius perspective of nucleation rates, where the expectation time for nucleation is written as $\bar{t} = \nu_0^{freq^{-1}} \exp(\Delta E^{total}/k_B T)$. ΔE^{total} represents the change in energy associated with the nucleating partial dislocation growing from its small equilibrium configuration to the nearby saddle configuration.

For simplicity, the nucleating dislocation segment was assumed to have a constant radius of curvature, r, and consist of three distinct energy components, $E^{total} = E^{ssf} + E^{disl} - W^{stress}$. E^{ssf} represents the energy of the stable stacking fault created by the partial dislocation segment, $E^{ssf} = \gamma_{ssf} A$, where A is the area swept by the nucleating dislocation segment. W^{stress} represents the interaction of the dislocation with the stress field created by the applied load, $W^{stress} = \int_A b_p^s \tau_{xy} ds$, where τ_{xy} corresponds to the xy shear stress field on the slip plane due to the applied load. The expression for τ_{xy} in an infinite elastic body containing a void is lengthy; thus, we refer the interested readers to [26] for brevity. b_p^s corresponds to the magnitude of the partial burgers vector in the $[1\bar{1}0]$ direction. E^{disl} represents the self energy of the nucleating dislocation segment and was taken to be

$$E^{disl} = \frac{\mu b_p^2 r}{8} \frac{2-\nu}{1-\nu} ln(\frac{4gr}{e^2 r_0}), \tag{3.3}$$

with μ being the shear modulus, b_p the magnitude of the partial dislocation burgers vector, ν the Poisson's ratio and r_0 the dislocation core cut-off radius. The function g captures the influence of void diameter, D, on the dislocation self energy,

$$g = 0.55 + \frac{\frac{4r}{e^2 r_0} - 0.55}{1 + \alpha(D)/r}. \tag{3.4}$$

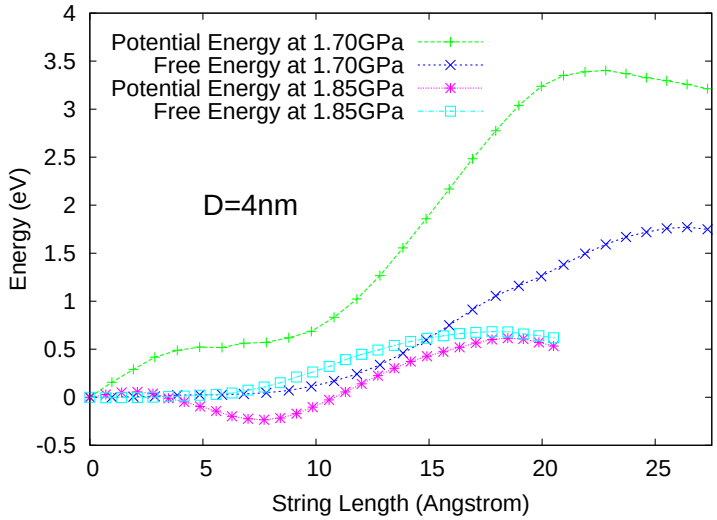

Figure 3.3: The potential and free energy profiles along the 300K principle curves [85] (strings) associated with partial dislocation nucleation from a spherical void at two fixed loadings. The considerable difference between the curves highlights the importance of entropy and indicates that the position of the principle curve in configuration space is significantly dependent upon load.

The form of g was chosen such that E^{disl} corresponds to the available analytic solutions for the two limiting cases of $r/D \to \infty$ (a full dislocation loop in an infinite elastic material [31]) and $r/D \to 0$ (a half dislocation loop at a free surface [6]) (see appendix B for more details). $\alpha(D)$ controls the rate at which E^{disl} transitions between these two solutions and was taken to be $\alpha(D) = c_2 D^2 + c_1 D$. Using $\mu = 69\text{GPa}$, $\nu = 0.33$, $r_0 = 1.1$, $b_p = 1.65$, $\gamma_{ssf} = 0.118\text{J/m}^2$, and $\nu_0^{freq} = 0.62\text{ps}^{-1}$, the continuum model was fit to the atomistic results for the $D = 4\text{nm}$ and $D = 6\text{nm}$ voids by setting $c_1 = 0.217$ and $c_2 = 0.079\text{nm}^{-1}$. The performance of the fit is demonstrated by its closeness with the atomistic simulation data for the $D \to \infty$ and $D = 8\text{nm}$ data in figure 3.2.

Together the atomistic simulations and analytic model suggest that dislocation nucleation will occur from spherical voids at far-field shear loadings of 0.9 to 2.0GPa at 300K depending upon the void size ($D > 4\text{nm}$) and the timescale

($\bar{t} < 1$yr), as shown in figure 3.2(b). For large voids, with diameters greater than 100nm, the nucleation load can be considered independent of size. For any particular void size, nucleation is highly unlikely at loads below $\sim 75\%$ of the critical load. Considering that all technologically relevant Al alloys have ultimate tensile strengths below 1GPa, the nucleation of dislocations from voids is predicted to be highly unlikely, unless the material is subjected to extreme shock loading [45] or voids are subjected to nanoscale stress concentrations such as other nearby dislocations.

With regard to mechanical testing, if dislocation nucleation from voids were to occur, the predictions suggest that the response would be considered relatively strain rate insensitive. Specifically, the strain rate sensitivity, $m = \partial ln\tau_f / \partial ln\dot{\gamma}$, associated with a material whose deformation is completely controlled by the nucleation of dislocations from voids, $\dot{\gamma} \propto k$, is predicted to be 0.004 at typical experimental timescales, with $\dot{\gamma}$ representing the shear strain rate and τ_f the shear flow strength. While this value is relatively independent of void size, it does depend upon the load/timescale at high (>ms^{-1}) nucleation rates, e.g. $m \approx 0.012$ at typical molecular dynamics rates (ns^{-1}). As a point of reference, mechanical testing of coarse grained polycrystalline Al, where deformation is controlled by dislocation-dislocation interactions, exhibits $m \approx 0.004$ [48].

3.5 Conclusions

In summary, we have combined atomistic modeling, variational TST, and a simple analytic model to predict dislocation nucleation rates from a spheri-

cal void in Al. Our findings suggest that nucleation is unlikely to occur under ordinary experimental conditions. This not only contributes to the ongoing debate regarding the mechanisms of nano-void growth and ductile failure [33, 70, 76, 2, 1, 44, 88, 79, 71, 72, 46, 47, 61, 77, 45], but also provides a prediction of the maximum attainable strength of Al alloys.

3.6 Acknowledgements

The authors acknowledge support from Paul Hess at ONR (Grant N00014-08-1-0862 and N00014-10-1-0323).

CHAPTER 4

COMPUTING THE RATES OF TRANSITION IN PRECIPITATE HARDENED AL-CU ALLOY

By Linh D. Nguyen and Derek H. Warner

4.1 Abstract

Precipitate hardening is known to be a process that contributes to yield strength of precipitate-strengthened alloys. Mechanisms controlling strength of interaction of dislocations and precipitates include cutting, looping, leading partial cutting with trailing partial looping, and diffusionless climb. This overlap makes the transition characteristics in precipitate hardened alloys at finite temperature so complex that transition flux concept with a linear distance reaction coordinate is not sufficient to capture the free energy profile. This work presents our attempts to study the complexity of transition in a precipitate problem though exploration of free energy information and transition rates. I show here that transition interface sampling (TIS) is a potential approach for the problem, that can predict transition rates with errors being in an order of magnitude.

4.2 Introduction

Introducing submicron precipitates into engineering alloys to hinder dislocation mobility has long been a popular technique to enhance the strength of underaged alloys. For many alloys, the precipitation is formed by nanometer-

size coherent metastable precipitates known as GP zones [62, 23]. Strengths of precipitation-hardened modern Al alloys can even reach the order of gigapascal [43, 82]. Understanding the controlling mechanisms associated with the interactions between dislocations and precipitates is crucial in predicting and improving the performance of such alloys. Several studies aimed to provide insights into the mechanisms [53, 18, 37, 55, 30, 36]. It is widely known that dislocations overcome precipitates via cutting and Orowan looping and, hypothetically, via formation of prismatic loops involving cross-slip and climb [28, 29]. Due to the submicron-scale dimension of the problem, atomistic simulation is a promising approach to help enrich our understanding of the dominant mechanisms of dislocation-precipitate interactions. Via some recent studies using atomistic simulation [74, 73], complexity of dislocation-precipitate interactions has been partially unveiled. However, investigations into the dynamics of transition in such systems at laboratory loads and temperatures, where thermal activation plays a significant role, is still lacking. At finite temperatures, variation in mechanisms becomes very important.

Here, interaction between a discrete dislocation and a single precipitate a simulation cell is studied via atomistic simulations, using different approaches to show the complexity in free energy landscape.

4.3 Transition Interface Sampling

In the second chapter, the study approach utilizing chain of states, with the FTS method for sampling, shows its value when probing the set of transition pathways, also called transition tube or reactive flux, and calculating the free energy

along the flux for dislocation nucleation problems. Those computations are performed on a simple reaction coordinate. In principle, for any system, the results given by a chain-of-state study should be independent of the choice of reaction coordinate. However, efficiency of sampling is very sensitive to definition of reaction coordinate. A bad choice of reaction coordinate can result in very large error when calculating free energy barrier. For very high dimensional systems in which multiple mechanisms are simultaneously operative, it is not feasible to find a suitable single reaction coordinate that can capture all characteristics of reactive transition. A simple 2D scenario for this possibility is schemed in figure 4.1. Transition in such a system can be rather split into two localized most probable paths represented by two wide arrows. Definition of a transition tube in this case becomes challenging or even inappropriate.

A different approach for overcoming the timescale problem without being sensitive to the choice of reaction coordinate is needed. Common sense tells us that a simulation method performing an importance sampling of true dynamical trajectories is relevant. The transition interface sampling (TIS) method [83] developed by Van Erp et al. is a potential candidate. With TIS, a reaction coordinate is also used to define a set of interfaces $\lambda_0, \lambda_1, \lambda_2, ..., \lambda_n$ between initial and final states. An interface in the configuration space λ_i is a multidimensional surface satisfying the condition that the value of chosen reaction coordinate be equal to a certain value, also denoted as λ_i. The set of values λ_i defining the set of interfaces must satisfy $\lambda_i < \lambda_{i+1}$. Configuration of the initial state A and final state B can be defined by the condition $\lambda \leqslant \lambda_0 = \lambda_A$ and $\lambda \geqslant \lambda_n = \lambda_B$, respectively. The transition rate is then expressed as

$$k_{AB} = f_A P_A(\lambda_B|\lambda_A), \tag{4.1}$$

with f_A being the rate at which the system escapes from the first interface λ_A

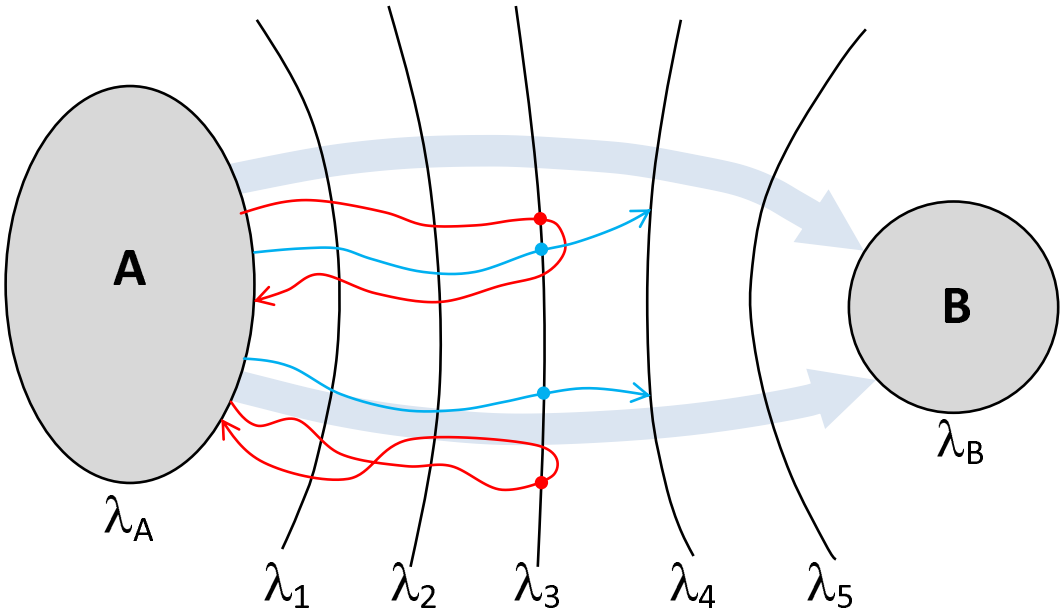

Figure 4.1: Illustration of a simple 2D scheme in which system transition from A to B tends to split to two separate fluxes represented by two wide arrows. Definition of a transition tube for the system by FTS method becomes unclear. Computation of transition rates using FTS methods is then unfeasible. TIS algorithm overcomes this challenge by performing statistics for blue-like and red-like trajectories for all pairs of interfaces λ_i, λ_{i+1} in order to calculate $P_A(\lambda_{i+1}|\lambda_i)$ used in equation 4.2.

toward the higher ones, and $P_A(\lambda_B|\lambda_A)$ the overall crossing probability. The flux f_A can be calculated via direct MD simulations. The later term is the probability that whenever the system crosses λ_A, it will cross λ_B before it crosses λ_A again. As λ_B is a surface at the other side of the barrier, this probability will be very small and cannot be calculated directly. This probability can, however, be determined by a series of path sampling simulations using the following factorization [83]:

$$P_A(\lambda_B|\lambda_A) = P_A(\lambda_n|\lambda_0) = \prod_{i=0}^{n-1} P_A(\lambda_{i+1}|\lambda_i) \tag{4.2}$$

Here, $P_A(\lambda_{i+1}|\lambda_i)$ is a probability quantity defined as follows: Given that a system just crossed λ_A more recently than λ_i, and it is going to cross λ_i in one time

step, $P_A(\lambda_{i+1}|\lambda_i)$ is the probability that the system will later on cross λ_{i+1} before getting back to λ_A (if that happens). $P_A(\lambda_{i+1}|\lambda_i)$ is visualized in figure 4.1 to be the ratio of the number of blue trajectories to the number of trajectories of both types, blue and red. It can be calculated reliably if we generate a large number of appropriate trajectories with correct statistical weight. Van Erp et al. proposed a Monte Carlo algorithm to perform this task. The detailed algorithm is shown in appendix C for reference. A trajectory that starts at λ_A and crosses λ_i at least once before ending at either λ_{i+1} or λ_A is required to start the algorithm. The starting point of a new trial trajectory for the next TIS step is picked from a random time slice of the previous full trajectory. The reaction rate k_{AB} calculated with TIS is often less sensitive to positions of the intermediate interfaces compared to other methods, such as FTS. The number of total interfaces and their positions only influence the efficiency of the method [83].

4.4 Simulation Setups

The atomistic simulations were conducted using a modified version LAMMPS package [58] and a recently developed AlCu empirical potential developed by Apostle and Mishin [3]. The potential is an angular dependent extension of the embedded atom method (EAM) [13, 51]. Based on a perfect fcc Al lattice, a monolayer precipitate was created by changing the atom type of selected Al atoms to Cu type. The simulation box (figure 4.2) contains approximately 13,000 atoms in total, with 13 Cu atoms in the precipitate. The box was bounded by $(1\bar{1}0)$, (111), and $(\overline{11}2)$ faces in the X, Y, and Z directions, respectively. The precipitate lies on the (100) plane. Periodic boundary conditions were applied in the X and Z directions. The Y surfaces were free and used to apply the load.

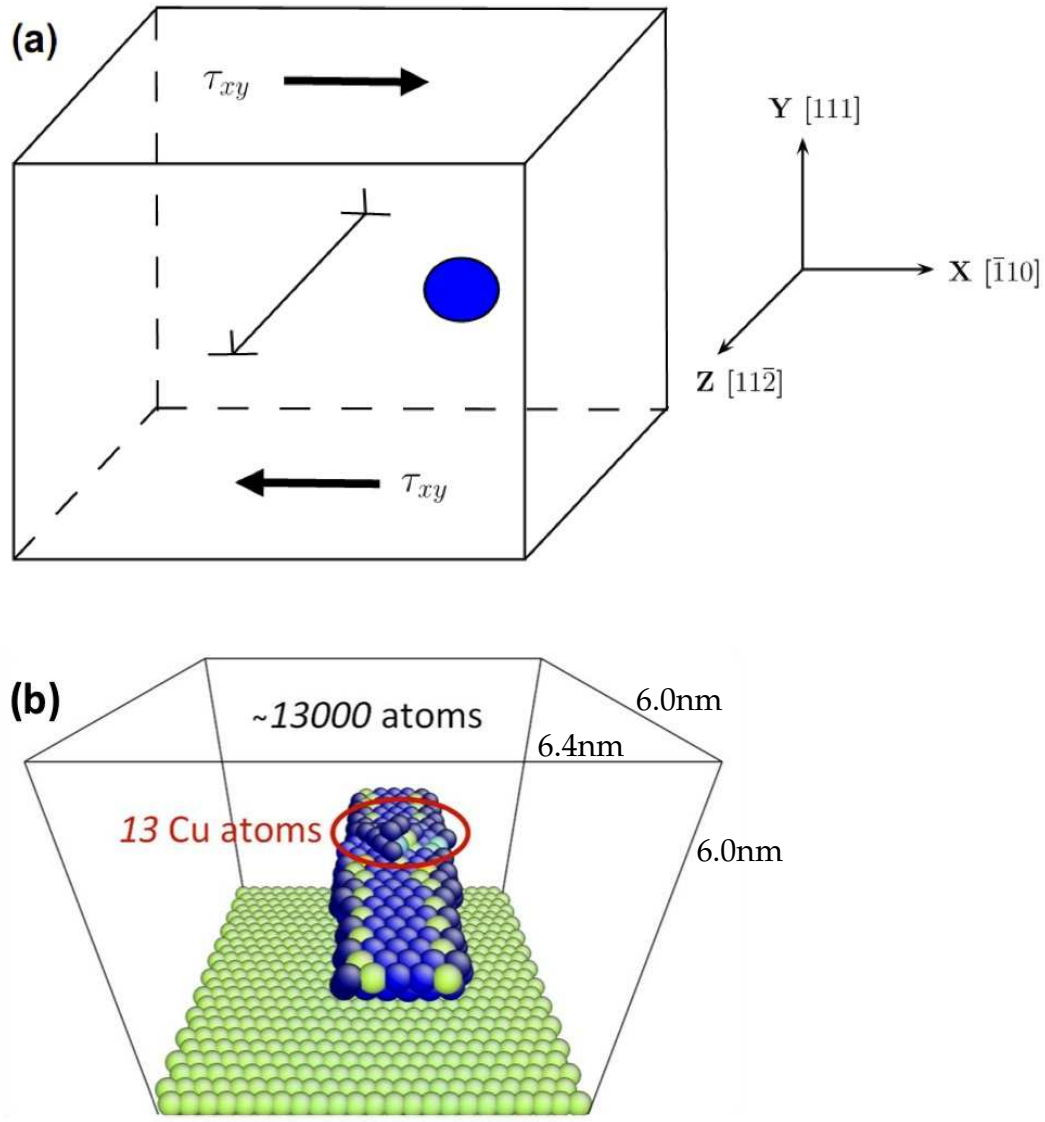

Figure 4.2: Simulation cell with an edge dislocation and a precipitate. (a) Lattice orientation and direction of shear load [74]; (b) The simulation cell configuration at 0K under zero load.

An edge dislocation was created with a line direction parallel to the Z-axis and $\vec{b} = 1/2[\bar{1}10]$. The Burgers vector of the edge dislocation lies in the (001) precipitate plane.

Direct MD simulations are performed with NPT dynamics. The system was

loaded by shearing two groups of atoms near the top and bottom Y surfaces. The constant traction in the X direction applied on each atom, either in the top or bottom group, is given by

$$f_{top} = \frac{\tau_{xy} A_{xz}}{N_{top}}, f_{bottom} = -\frac{\tau_{xy} A_{xz}}{N_{bottom}}, \tag{4.3}$$

where τ_{xy} is the applied shear stress, A_{xz} is the surface area, and N_{top}, N_{bottom} are the number of atoms on the top and bottom surfaces, respectively.

FTS computations are initialized from snapshots captured in direct MD simulations. Shear forces were adjusted accordingly in order to obtain desired loads at which FTS and TIS sampling are performed. The strings computed in FTS were employed to define sets of interfaces based on which TIS simulations are performed. The string computed by the FTS method for a simulation cell is used as a successful path to start the corresponding TIS simulation.

The reaction coordinate for all cases of study presented in this dissertation is chosen to be Cartesian distance in high-dimension configurational space. With this choice, the distance between two states i and j is given

$$d^{ij} = \sqrt{\sum_{k=1}^{3N} (x_k^i - x_k^j)^2}, \tag{4.4}$$

with x being the Cartesian coordinates (x, y, or z) of atoms and N the total number of atoms. The sum is taken over all degrees of freedom.

The set of interfaces for TIS is simply defined as the boundaries between Voronoi cells of convergent strings, given by the FTS method. Simulations to compute $P_A(\lambda_{i+1}|\lambda_i)$ for each λ_i are performed independently. For each λ_i, we perform five simulations, in parallel, and with different random seeds, in 1ns. Then, the total simulation time for computing each of $P_A(\lambda_{i+1}|\lambda_i)$ is 5ns. For

each TIS rate computation, transition flux through the first interface is calculated from 50 independent direct MD simulations at 300K, with different random seeds.

4.5 Results and Discussion

4.5.1 Chain of States Study

With the same choice of reaction coordinate, the FTS method shows its performance in the second and third chapters when studying dislocation nucleation problems. For the dislocation-precipitate interaction problem, however, FTS method holds all the drawbacks of the reaction coordinate definition. FTS method based on the chosen reaction coordinate shows a disability to capture free energy profile of system transition. Table 4.1 shows the results given by different TST approaches that are already introduced in the second chapter.

Method	expectation time(ns)	energy barrier(eV)
Direct MD	2.5	-
0K harmonic TST	3.5×10^{19}	1.23
expanded lattice hTST	1.4×10^{17}	1.28
PMF (string computation)	2.8×10^{7}	0.60
FTS flux (fixed string)	N/A	N/A

Table 4.1: Expectation time predictions and energetics associated with transition in the precipitate hardening simulation cell at 300K, under shear load of 200MPa, using MD vs. TST-based approaches.

Complexity of transition in the system is showed clearly in the table 4.1 with huge errors in predictions by chain-of-state approaches. Compared to their performance for the 2D nucleation problem, the errors for this precipitate problem

magnifies by several orders of magnitude. Our efforts to estimate a free energy barrier profile at finite temperature is frustrated. The FTS sampling, although in its first stage can result in a convergent string, is unable to obtain a stable flux matrix of transition when running simulation with the string fixed. There are two possibilities that could explain the observed poor performance. First, uniqueness for the convergent string representing the most probable path is not certain. Second, even if it is possible to obtain a convergent string that is independent of the starting string, convergence for flux matrix is not guaranteed.

Procedures of the FTS method deserve comment in this case. In the first stage of FTS when string is being computed, whenever the system associated with a certain Voronoi cell escapes from that cell, the FTS algorithm brings it back to the current position of the cell center. In our opinion, this can be a biased treatment in some cases. Following are two possible scenarios. First, the resulting convergent string in this case is dependent of the starting string. The string may eventually convert toward different paths depending on where it starts from (similar to scheme in figure 4.1). In dislocation nucleation problems, we neglect this possibility because when a string is fixed to run sampling for flux we observe convergence of free energy profile which is in accordance with the string. Second, given that an independent convergent string is obtainable, flux matrix obtained in the next stage may not physically reflect most of the possible transition path in the system. It is possible that once a system is trapped into a certain zone apart from the fixed string, the system will spend most of its time in that zone which is far from system's cell center, as well as centers of neighbor cells. Confining the systems in their associate Voronoi cells to compute for free energy profile is reliable only if average sampling positions of neighbor systems can be connected smoothly and without any unphysical discontinuity.

4.5.2 Transition Interface Sampling Study

Method	2D nucleation	Precipitation
Direct MD	17ns	2.5ns
FTS	13ns	N/A
TIS	8ns	0.4ns

Table 4.2: Expectation time (inverse of rate) predictions by FTS vs. TIS for 2D dislocation nucleation problem at 1.1 GPa (chapter 2) and precipitate problem at 200MPa. $P_A(\lambda_{i+1}|\lambda_i)$ for each λ_i is computed based on 5ns simulations.

Table 4.2 shows the expectation times of transition predicted by TIS, in comparison to the results by FTS method, for 2D dislocation nucleation and precipitate problem. With respect to the expectation times given by direct MD simulations, the FTS prediction shows higher accuracy than the TIS prediction for 2D nucleation problem. For the precipitate problem, however, FTS method fails to measure free energy barriers, although convergent strings are observed after the first stage of the FTS sampling. With TIS, the rate of transition is overestimated by approximately an order of magnitude.

Figure 4.3 presents the TIS results for the precipitate problem at three different loads of 150MPa, 180MPa, and 200MPa. In contradiction to the case of 200MPa, the TIS, at 180MPa, underestimates the transition rate, compared to the MD result (figure 4.3(a)). The error is still in an order of magnitude. The difference in the signs of errors observed for the two loads, and the consistency in their magnitude, suggest that the error in TIS is potentially random error. The predictions, hence, can be improved with enhanced randomness in simulation.

For such complex transition as in the precipitate problem, the choice of the last cell, $n-1$, to calculate the rate k_{AB} with equation 4.2 is unclear. Fortunately, we observe here that each calculated expectation time reaches its maximum

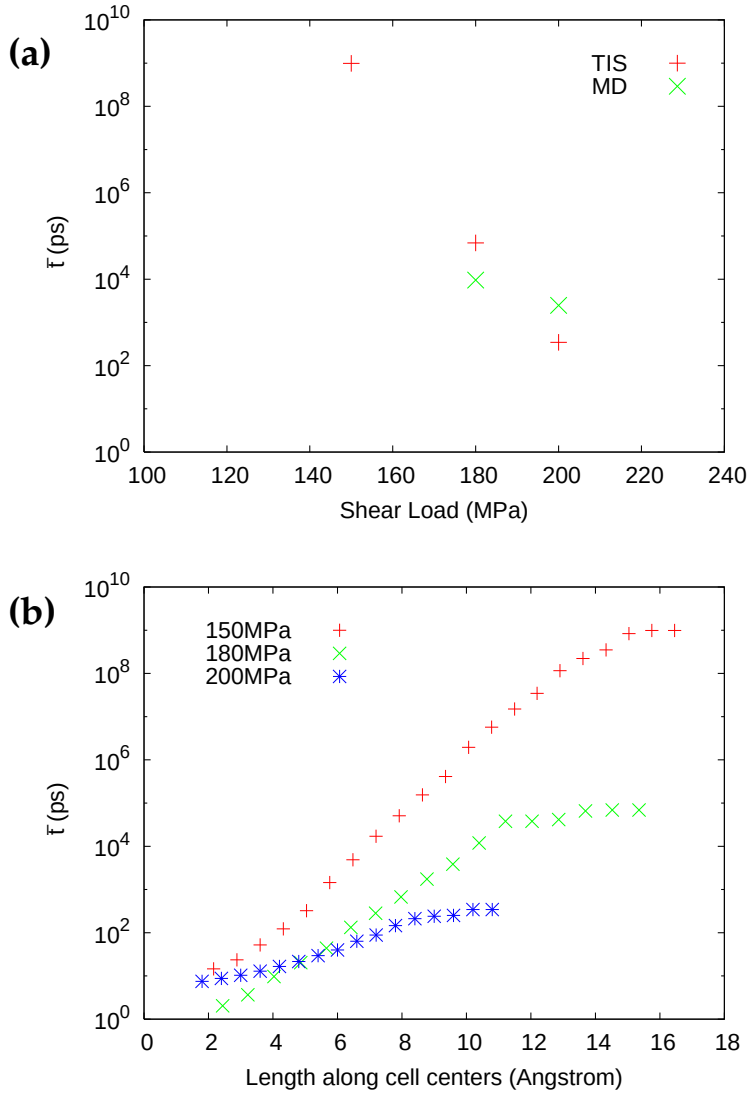

Figure 4.3: (a) Comparison of MD simulation times and TIS predicted times at high loads. (b) The expectation times predicted by TIS for the precipitate system at different loads. $\bar{t}$ shows convergence when additional interfaces on the side of reactive direction are taken into account. Interfaces are marked via Voronoi cells.

value at a certain interface, $n-1$, and will not change significantly when more interfaces are included in the computation. This means $P_A(\lambda_{i+1}|\lambda_i) \to 1$ when λ_i surpasses a certain interface. Intuitively, the interface (we mark interfaces via Voronoi cells) where we start to see saturation should already passes the saddle interface, assuming that such saddle interface can be defined. Unreasonable choice for set of interfaces may not result in sharp saturation.

4.6 Conclusions

For a simulation cell that balances between computation expense and complexity representation, we conduct a case study for interaction between dislocation and precipitate in Al-Cu alloys, in the context of transition rates computation. Variation of the results given by different approaches reveal the complexity in the system's free energy landscape. The FTS method, with a typical reaction coordinate, is inadequate to provide variational TST rate prediction for the problem. However, information given by FTS sampling can be used as a reasonable choice for set of interfaces needed to perform TIS. TIS algorithm, while short of tool to obtain free energy profile of transition, can compute the rates of transition with an error approximately in an order of magnitude, in reasonable simulation time. This work serves to contribute information for future atomistic simulation studies on more realistic precipitate hardened problems.

4.7 Acknowledgements

The authors acknowledge support from Paul Hess at ONR (Grant N00014-08-1-0862 and N00014-10-1-0323).

APPENDIX A

ALGORITHM OF THE MOST RECENT VERSION OF THE FTS METHOD

Following is the algorithm for the newest version of the FTS method, developed by Vanden-Eijnden and Venturoli [85]. Let us consider a system whose dynamics is governed by the following overdamped Langevin equation:

$$\dot{\mathbf{x}}(t) = -\nabla V(\mathbf{x}(t)) + \sqrt{2\beta^{-1}}\boldsymbol{\eta}(t), \tag{A.1}$$

with $V(\mathbf{x})$ being the potential energy, $\beta = 1/(k_B T)$ the inverse temperature, $\boldsymbol{\eta}(t)$ a Gaussian white noise with mean zero and covariance $\langle \eta_i(t)\eta_j(t)\rangle = \delta_{ij}\delta(t-t')$. We have used units of time such that the friction coefficient is 1 in these units. The procedures basically include five steps:

1. Update $\mathbf{x}_\alpha^n$ via a time-discretized version of overdamped Langevin equation A.1 with a reflecting boundary condition at the boundary of the Voronoi cell associated with the image $\boldsymbol{\varphi}_\alpha^n$. For example, calculate

$$\mathbf{x}_\alpha^* = \mathbf{x}_\alpha^n - \Delta t \nabla V(\mathbf{x}_\alpha^n) + \sqrt{2\beta^{-1}\Delta t}\boldsymbol{\xi}_\alpha^n, \tag{A.2}$$

and set $\mathbf{x}_\alpha^{n+1} = \mathbf{x}_\alpha^*$, if $\mathbf{x}_\alpha^* \in \mathbf{B}_\alpha^n$, and $\mathbf{x}_\alpha^{n+1} = \mathbf{x}_\alpha^n$ otherwise, where $\mathbf{B}_\alpha^n = \{\mathbf{x}\}$ such that $|\mathbf{x} - \boldsymbol{\varphi}_\alpha^n| < |\mathbf{x} - \boldsymbol{\varphi}_{\alpha'}^n|$ for all $\alpha' \neq \alpha$.

In equation A.2, Δt denotes the time step used for numerical integration of equation A.1 and $\boldsymbol{\xi}_\alpha^n$ are independent Gaussian variables with mean 0 and variance 1.

2. Compute the running average of each $\mathbf{x}_\alpha^n$,

$$\bar{\mathbf{x}}_\alpha^n = \frac{1}{n}\sum_{n'=0}^{n} \mathbf{x}_\alpha^{n'} \tag{A.3}$$

3. Update each image along the string toward the running average $\bar{\mathbf{x}}_\alpha^n$ while keeping the string smooth. To do so use

$$\boldsymbol{\varphi}_\alpha^* = \boldsymbol{\varphi}_\alpha^n - \Delta\tau(\boldsymbol{\varphi}_\alpha^n - \bar{\mathbf{x}}_\alpha^n) + \mathbf{r}_\alpha^*, \tag{A.4}$$

where $\Delta\tau > 0$, $\mathbf{r}_0^* = \mathbf{r}_N^* = 0$, and for $\alpha = 1, 2, ..., N-1$,

$$\mathbf{r}_\alpha^* = \kappa^n(\boldsymbol{\varphi}_{\alpha+1}^* + \boldsymbol{\varphi}_{\alpha-1}^* - 2\boldsymbol{\varphi}_\alpha^*). \tag{A.5}$$

Here $\kappa^n > 0$ is an adjustable parameter that controls how aggressive the smoothing is.

4. Enforce the equal arc-length parametrization by interpolating a piecewise linear curve through $\{\boldsymbol{\varphi}_\alpha^*\}_{\alpha=0,...,N}$ and redistributing points at equal distance along this curve to obtain $\left\{\boldsymbol{\varphi}_\alpha^{n+1}\right\}_{\alpha=0,...,N}$.

5. If $\mathbf{x}_\alpha^{n+1} \in \mathbf{B}_\alpha^{n+1}$ go to step 1, otherwise set $\mathbf{x}_\alpha^{n+1} = \boldsymbol{\varphi}_\alpha^{n+1}$ and go to step 1. Repeat until convergence of $\left\{\boldsymbol{\varphi}_\alpha^{n+1}\right\}_{\alpha=0,...,N}$.

APPENDIX B

ELASTIC SELF-ENERGY MODEL FOR A DISLOCATION LOOP NUCLEATING FROM A SPHERICAL VOID

In the Beltz-Freund model [6], a constant geometry correction factor g independent of loop size is introduced into Hirth-Lothe's elastic self-energy analytical solution for a full circular dislocation loop [31] (equation B.1) to obtain a solution for the energy of a half loop (equation B.2) nucleating from a free surface. Following are the expressions for those two cases:

$$U^{full} = \frac{\mu b^2 r}{4} \frac{2-\nu}{1-\nu} ln(\frac{4r}{e^2 r_0}) \tag{B.1}$$

$$U^{half} = \frac{\mu b^2 r}{8} \frac{2-\nu}{1-\nu} ln(\frac{4gr}{e^2 r_0}), \tag{B.2}$$

with r being the loop/half loop radius, μ the shear modulus, b the Burgers vector, ν Poisson's ratio and r_0 the core cut-off radius.

It should be noticed that a loop nucleating from a void has similar geometry to a loop nucleating from a flat surface when loop size is significantly smaller than void size, and that the geometry changes when the loop grows and eventually has the form of a circular full loop. From that observation, we make correction by introducing a varying geometry factor g to the Beltz-Freund model. Apparently, g must be a function of void size and loop size. For any void size, the bound values of g when $D \approx 0$ and $D \to \infty$ must be the value for half loop, $g^{half} = 0.55$, and the value to match equation B.2 with equation B.1, $g^{full} = \frac{4R}{e^2 r_0}$, respectively. Analytic form of g is then constructed as follows:

$$g = g^{half} + \frac{1}{1 + \alpha(a)/D}(g^{full} - g^{half}), \tag{B.3}$$

with $\alpha(a)$ being a positive function of void radius a. The form of $\alpha(a)$ determines how quick a loop changes its behavior from "half-loop" to "full-loop" when it grows. We observed that $\alpha(a)$ can be well desribed via a quadratic function of void radius, $\alpha(a) = c_2D^2 + c_1D + c_0$, to match the model with our V-TST results once the core cut-off radius r_0 is chosen appropriately. Our problems here prefer $r_0 = 1.1$. The parameter c_0 must be 0 since $\alpha(a)$ should in principle be 0 for the limit case of very small voids. Fitting for the V-TST results from voids of diameters $D = 4$nm and $D = 6$nm gives us $c_1 = 0.217$ and $c_2 = 0.079nm^{-1}$.

APPENDIX C

TIS SHOOTING ALGORITHM

The following scheme (figure C.1) illustrates the shooting algorithm in TIS developed by Van Erp et al. [83]. The panels (a) through (l) depict trajectories/trajectory-segments on a free energy surface. The dashed horizontal lines are the TIS interfaces ($n = 4$ and $i = 2$ in this case). The algorithm requires an initial path (a) to start the loop. The length of this particular path $L^{(o)}$ is eighteen time slices (end points are not included). At step I, a random point is picked from this old path and some small randomized changes are applied to the velocities of all the particles (II), followed by a Metropolis acceptance/rejection step (III). In (c), the new velocities have resulted in a much larger kinetic energy $E^{(n)}$ and therefore this trial move is most likely rejected. Step IV is required to maintain detailed balance between pathways of different lengths. For example, if the random number generator assigns $\alpha = 0.59$ then $L^{max} = 30$, and we can reject when the path is unfinished but already contains 31 time slices as in panel (f) and (i). At (V), the equations of motion are integrated backwards in time by a MD algorithm using the shooting point with reverse velocities as starting point. At (VI) the equations of motion are integrated forward in time, starting from the same shooting point (without reversed velocities). After a rejection the old path is kept and counted again. If accepted, the new path will automatically start at λ_A and cross λ_i. The path can end at either λ_A as in (j) or at λ_{i+1} as in (k). The fraction of sampled pathways that end at λ_{i+1} determines $P_A(\lambda_{i+1}|\lambda_i)$.

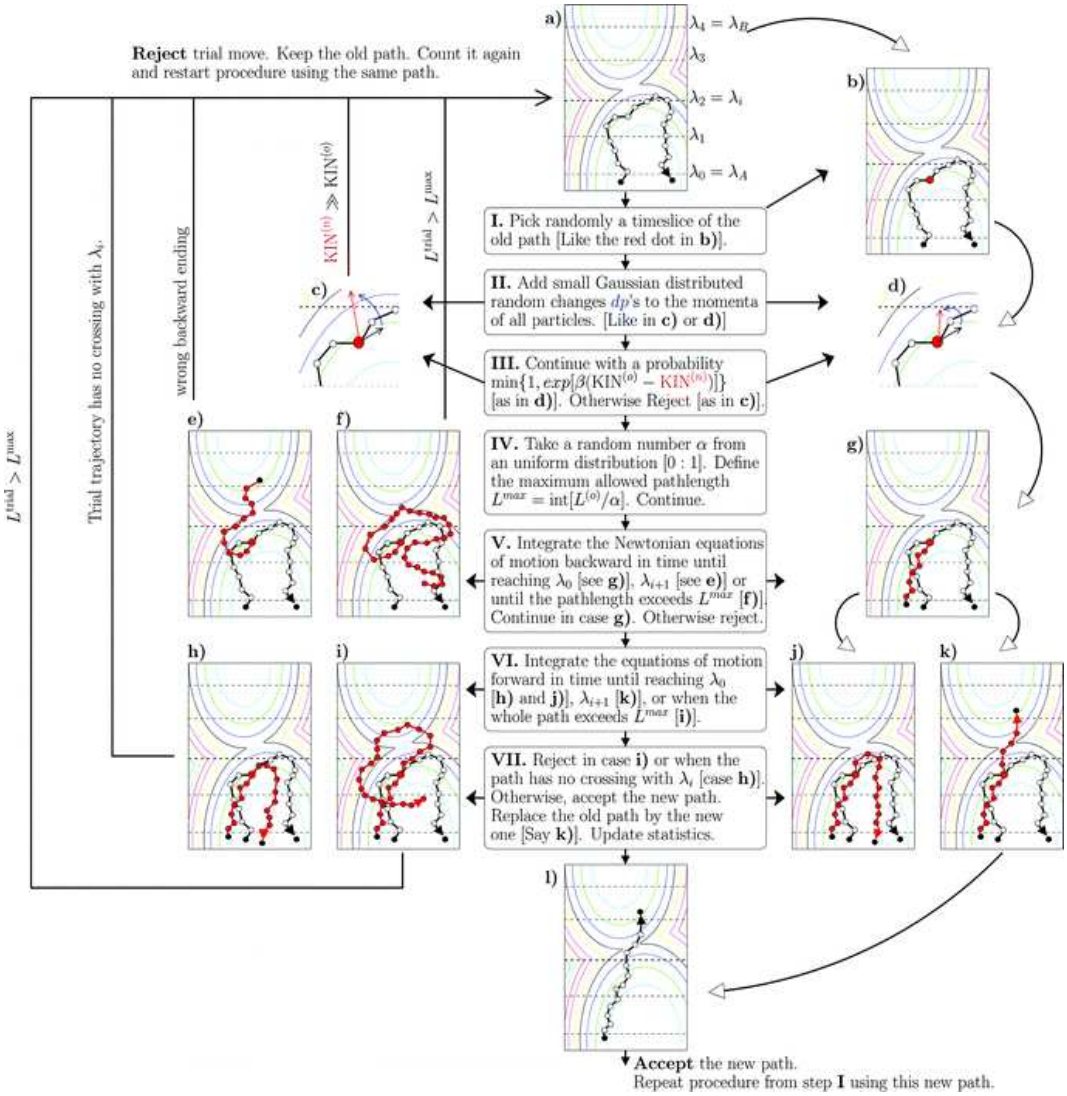

Figure C.1: Illustration of the TIS algorithm steps [83].

BIBLIOGRAPHY

[1] D. Ahn, P. Sofronis, and R. Minich. On the micromechanics of void growth by prismatic-dislocation loop emission. *Journal of the Mechanics and Physics of Solids*, 54(4):735–755, April 2006.

[2] D. C. Ahn, P. Sofronis, M. Kumar, J. Belak, and R. Minich. Void growth by dislocation-loop emission. *Journal of Applied Physics*, 101(6):063514, 2007.

[3] F. Apostle and Y. Mishin. Al-cu potential. *unpublished*, unpublished.

[4] T. Bartsch, T. Uzer, J. M. Moix, and R. Hernandez. Transition-state theory rate calculations with a recrossing-free moving dividing surface. *The Journal of Physical Chemistry B*, 112(2):206–212, January 2008.

[5] R. Becker and W. Doring. The kinetic treatment of nuclear formation in supersaturated vapors. *Annals of Physics*, 416(8):719–752, 1935.

[6] G. E. Beltz and L. B. Freund. On the nucleation of dislocations at a crystal surface. *Physica Status Solidi B*, 180(2):303, 1993.

[7] G. R. Bowman, V. A. Voelz, and V. S. Pande. Taming the complexity of protein folding. *Current Opinion in Structural Biology*, 21(1):4–11, February 2011.

[8] C. Brandl, P. M. Derlet, and H. Van Swygenhoven. Strain rates in molecular dynamics simulations of nanocrystalline metals. *Philosophical Magazine*, 89(34):3465–3475, 2009.

[9] E. M. Bringa, S. Traiviratana, and M. A. Meyers. Void initiation in fcc metals: Effect of loading orientation and nanocrystalline effects. *Acta Materialia*, 58(13):4458–4477, August 2010.

[10] V. V. Bulatov, W. G. Wolfer, and M. Kumar. Shear impossibility: Comments on "void growth by dislocation emission" and "void growth in metals: Atomistic calculations". *Scripta Materialia*, 63(1):144–147, July 2010.

[11] Srinath S. Chakravarthy and W. A. Curtin. Stress-gradient plasticity. *Proceedings of the National Academy of Sciences*, 108(38):15716–15720, September 2011.

[12] D. Chandler. Statistical mechanics of isomerization dynamics in liquids and the transition state approximation. *The Journal of Chemical Physics*, 68(6):2959–2970, 1978.

[13] Murray S. Daw and M. I. Baskes. Embedded-atom method: Derivation and application to impurities, surfaces, and other defects in metals. *Physical Review B*, 29(12):6443 LP – 6453, 1984.

[14] P. M. Derlet, P. Gumbsch, R. Hoagland, J. Li, D. L. McDowell, H. Van Swygenhoven, and J. Wang. Atomistic simulations of dislocations in confined volumes. *MRS Bulletin*, 2009.

[15] H. Eyring. The activated complex in chemical reactions. *The Journal of Chemical Physics*, 3(2):107–115, 1935.

[16] F. D. Fischer and T. Antretter. Deformation, stress state and thermodynamic force for a growing void in an elasticplastic material. *International Journal of Plasticity*, 25(10):1819–1832, October 2009.

[17] N. A. Fleck and J. W. Hutchinson. A phenomenological theory for strain gradient effects in plasticity. *Journal of the Mechanics and Physics of Solids*, 41(12):1825–1857, December 1993.

[18] V. Gerold and Haberkorn. *Phys. Status Solidi*, 16:675, 1966.

[19] D. Gianola, D. Warner, J. Molinari, and K. Hemker. Increased strain rate sensitivity due to stress-coupled grain growth in nanocrystalline al. *Scripta Materialia*, 55(7):649–652, October 2006.

[20] J. J. Gilman. Dislocation sources in crystals. *Journal of Applied Physics*, 30(10):1584–1594, 1959.

[21] S. Glasstone, K. J. Laidler, and H. Eyring. *The Theory of Rate Processes*, volume 19. May 1942.

[22] P. A. Gordon, T. Neeraj, and M. J. Luton. Atomistic simulation of dislocation nucleation barriers from cracktips in alpha-fe. *Modelling and Simulation in Materials Science and Engineering*, 16(4):045006, June 2008.

[23] A. Guinier. *Ann. Phys.*, 12:161, 1939.

[24] A. L. Gurson. Continuum theory of ductile rupture by void nucleation and growth, 1. yield criteria and flow rules for porous ductile media. *Journal of Engineering Materials and Technology-Transactions of the ASME 99(1)*, pages 2–15, 1977.

[25] S. Hara and J. Li. Adaptive strain-boost hyperdynamics simulations of stress-drivenatomic processes. *Physical Review B*, 82(18):184114, November 2010.

[26] L. He and Z. Li. Impact of surface stress on stress concentration. *International Journal of Solids and Structures*, 43(20):6208–6219, October 2006.

[27] P. Hirel, J. Godet, S. Brochard, L. Pizzagalli, and P. Beauchamp. Determination of activation parameters for dislocation formation from a surface in fcc metals by atomistic simulations. *Physical Review B*, 78(6):064109, August 2008.

[28] P. B. Hirsch. The interpretation of the slip pattern in terms of dislocation movements. *J Inst Metals*, 86:13–14, 1957.

[29] P. B. Hirsch and F. J. Humphreys. The deformation of single crystals of copper and copper-zinc alloys containing alumina particles. i. macroscopic properties and workhardening theory. *Proceedings of the Royal Society of London. Series A, Mathematical and Physical Sciences*, 318(1532):45–72, 1970.

[30] P. B. Hirsch and A. Kelly. *Philosophical Magazine*, 12:881, 1965.

[31] J. P. Hirth and J. Lothe. *Theory of Dislocations*. McGraw-Hill, 1968.

[32] J. Horiuti. On the statistical mechanical treatment of the absolute rate of chemical reaction. *Bulletin of the Chemical Society of Japan*, 13:210–213, 1938.

[33] M. Huang, Z. Li, and C. Wang. Discrete dislocation dynamics modelling of microvoid growth and its intrinsic mechanism in single crystals. *Acta Materialia*, 55(4):1387–1396, February 2007.

[34] C. Jin, W. Ren, and Y. Xiang. Computing transition rates of thermally activated events in dislocation dynamics. *Scripta Materialia*, 62(4):206–209, February 2010.

[35] J. C. Keck. Statistical investigation of dissociation cross-sections for diatoms. *Discuss. Faraday Soc.*, 33:173–182, 1962.

[36] A. Kelly. Theories of precipitation and dispersion hardening. In *Electron Microscopy and Strength of Crystals*, pages 947–971. John Wiley and Sons, 1963.

[37] G. Knowles and P. M. Kelly. Effect of second phase particles on the mechanical properties of steel. In *BSC/ISI Conference, Scarborough, The Iron and Steel Institute, London*, page 9, 1971.

[38] U. F. Kocks, A. S. Argon, and M. F. Ashby. *Themodynamics and Kinetics of Slip*. 1975.

[39] K. S. Kumar, H. Van Swygenhovenb, and S. Sureshc. Mechanical behavior of nanocrystalline metals and alloys. *Acta Materialia*, 51(19):5743–5774, November 2003.

[40] M. Legros, F. Mompiou, D. S. Gianola, A. Sedlmayr, O. Kraft, and D. Caillard. Mechanical strength and deformation modes of sub-micron al fibers. *Submitted*, 2010.

[41] J. Li. Atomeye: An efficient atomistic configuration viewer. *Modelling and Simulation in Materials Science and Engineering*, 11(2):173–177, March 2003.

[42] L. Li, P. Anderson, M. Lee, E. Bitzek, P. Derlet, and H. Swygenhoven. The stress- strain response of nanocrystalline metals: A quantized crystal plasticity approach. *Acta Materialia*, 57(3):812–822, February 2009.

[43] Peter V. Liddicoat, Xiao-Zhou Liao, Yonghao Zhao, Yuntian Zhu, Maxim Y. Murashkin, Enrique J. Lavernia, Ruslan Z. Valiev, and Simon P. Ringer. Nanostructural hierarchy increases the strength of aluminium alloys. *Nature Communications*, 1(6):1–7, September 2010.

[44] V. A. Lubarda. Emission of dislocations from nanovoids under combined loading. *International Journal of Plasticity*, 27(2):181–200, February 2011.

[45] V. A. Lubarda, M. S. Schneider, D. H. Kalantar, B. A. Remington, and M. A. Meyers. Void growth by dislocation emission. *Acta Materialia*, 52(6):1397–1408, April 2004.

[46] J. Marian, J. Knap, and M. Ortiz. Nanovoid cavitation by dislocation emission in aluminum. *Physical Review Letters*, 93(16):165503, Oct 2004.

[47] J. Marian, J. Knap, and M. Ortiz. Nanovoid deformation in aluminum under simple shear. *Acta Materialia*, 53(10):2893–2900, June 2005.

[48] J. May, H. Hoppel, and M. Goken. Strain rate sensitivity of ultrafine-grained aluminium processed by severe plastic deformation. *Scripta Materialia*, 53(2):189–194, July 2005.

[49] R. Meana-Paneda, D. G. Truhlar, and A. F. Ramos. High-level direct-dynamics variational transition state theory calculations including multi-dimensional tunneling of the thermal rate constants, branching ratios, and kinetic isotope effects of the hydrogen abstraction reactions from methanol by atomic hydrogen. *The Journal of Chemical Physics*, 134(9):094302, 2011.

[50] Y. Mishin, D. Farkas, M. J. Mehl, and D. A. Papaconstantopoulos. Interatomic potentials for monoatomic metals from experimental data and ab initio calculations. *Physical Review B*, 59(5):3393–3407, Feb 1999.

[51] Y. Mishin, M. J. Mehl, and D. A. Papaconstantopoulos. Phase stability in the fe-ni system: Investigation by first-principles calculations and atomistic simulations. *Acta Materialia*, 53:4029–4041, 2005.

[52] Y. Mishin, M. R. Sorensent, and A. F. Voter. Calculation of point-defect entropy in metals. *Philosophical Magazine A*, 81(11):2591–2612, 2001.

[53] N. F. Mott and F. R. N. Nabarro. Report of a conference on the strength of solids. page 1. The Physical Society, London, 1948.

[54] A. K. Nair, D. H. Warner, R. G. Hennig, and W. A. Curtin. Coupling quantum and continuum scales to predict crack tip dislocation nucleation. *Scripta Materialia*, 63(12):1212–1215, December 2010.

[55] E. Nembach. Precipitation hardening caused by a difference in shear modulus between particle and matrix. *Physica Status Solidi (a)*, 78:571–581, 1983.

[56] L. D. Nguyen, K. L. Baker, and D. H. Warner. Atomistic predictions of dislocation nucleation with transition state theory. *Physical Review B*, 84(2):024118, July 2011.

[57] F. Noe, I. Horenko, C. Schutte, and J. C. Smith. Hierarchical analysis of conformational dynamics in biomolecules: Transition networks of metastable states. *The Journal of Chemical Physics*, 126(15):155102, April 2007.

[58] S. Plimpton. Fast parallel algorithms for short-range molecular dynamics. *J. Comput. Phys.*, 117:1–19, March 1995.

[59] E. Pollak and P. Talkner. Transition-state recrossing dynamics in activated rate processes. *Physical Review E*, 51(3):1868–1878, March 1995.

[60] E. Pollak and P. Talkner. Reaction rate theory: What it was, where is it today, and where is it going? *Chaos: An Interdisciplinary Journal of Nonlinear Science*, 15(2):026116, 2005.

[61] G. P. Potirniche, M. F. Horstemeyer, G. J. Wagner, and P. M. Gullett. A molecular dynamics study of void growth and coalescence in single crystal nickel. *International Journal of Plasticity*, 22(2):257–278, February 2006.

[62] G. D. Preston. *Philosophical Magazine*, 26:855, 1938.

[63] J. R. Rice and G. E. Beltz. The activation energy for dislocation nucleation at a crack. *Journal of the Mechanics and Physics of Solids*, 42(2):333–360, February 1994.

[64] J. R. Rice and R. Thomson. Ductile versus brittle behaviour of crystals. *Philosophical Magazine*, 29(1):73–97, 1974.

[65] J. R. Rice and D. M. Tracey. On the ductile enlargement of voids in triaxial stress fields*. *Journal of the Mechanics and Physics of Solids*, 17(3):201–217, June 1969.

[66] G. Richter, K. Hillerich, D. S. Gianola, R. Monig, O. Kraft, and C. A. Volkert. Ultrahigh strength single crystalline nanowhiskers grown by physical vapor deposition. *Nano Letters*, 9(8):3048–3052, August 2009.

[67] D. Rodney. Activation enthalpy for kink-pair nucleation on dislocations: Comparison between static and dynamic atomic-scale simulations. *Physical Review B*, 76(14):144108, Oct 2007.

[68] Seunghwa Ryu, Keonwook Kang, and Wei Cai. Entropic effect on the rate of dislocation nucleation. *Proceedings of the National Academy of Sciences*, 108(13):5174–5178, March 2011.

[69] T. Schneider and E. Stoll. Molecular-dynamics study of a three-dimensional one-component model for distortive phase transitions. *Physical Review B*, 17(3):1302–1322, Feb 1978.

[70] J. Segurado and J. Llorca. An analysis of the size effect on void growth in single crystals using discrete dislocation dynamics. *Acta Materialia*, 57(5):1427–1436, March 2009.

[71] E. T. Seppala, J. Belak, and R. E. Rudd. Effect of stress triaxiality on void growth in dynamic fracture of metals: A molecular dynamics study. *Physical Review B*, 69(13):134101, April 2004.

[72] E. T. Seppala, J. Belak, and R. E. Rudd. Three-dimensional molecular dynamics simulations of void coalescence during dynamic fracture of ductile metals. *Physical Review B*, 71(6):064112, February 2005.

[73] C. V. Singh, A. J. Mateos, and D. H. Warner. Atomistic simulations of dislocation-precipitate interactions emphasize importance of cross-slip. *Scripta Materialia*, 64(5):398–401, March 2011.

[74] C. V. Singh and D. H. Warner. Mechanisms of GuinierPreston zone hardening in the athermal limit. *Acta Materialia*, 58(17):5797–5805, October 2010.

[75] N. Singhal, C. D. Snow, and V. S. Pande. Using path sampling to build better markovian state models: Predicting the folding rate and mechanism of a tryptophan zipper beta hairpin. *The Journal of Chemical Physics*, 121(1):415–425, July 2004.

[76] M. B. Taylor, H. M. Zbib, and M. A. Khaleel. Damage and size effect during superplastic deformation. *International Journal of Plasticity*, 18(3):415–442, March 2002.

[77] S. Traiviratana, E. M. Bringa, D. J. Benson, and M. A. Meyers. Void growth in metals: Atomistic calculations. *Acta Materialia*, 56(15):3874–3886, September 2008.

[78] D. G. Truhlar and B. C. Garrett. Variational transition state theory. *Annual Review of Physical Chemistry*, 35(1):159–189, 1984.

[79] T. Tsuru and Y. Shibutani. Initial yield process around a spherical inclusion in single-crystalline aluminium. *Journal of Physics D: Applied Physics*, 40(7):2183–2188, April 2007.

[80] T. C. Tszeng. Threshold condition of dislocation loop emission from microvoids. *Journal of Applied Physics*, 103(5):053509, 2008.

[81] B. P. Uberuaga, R. G. Hoagland, A. F. Voter, and S. M. Valone. Direct transformation of vacancy voids to stacking fault tetrahedra. *Physical Review Letters*, 99(13):135501, September 2007.

[82] R. Z. Valiev, N. A. Enikeev, Murashkin, V. U. Kazykhanov, and X. Sauvage. On the origin of the extremely high strength of ultrafine-grained al alloys produced by severe plastic deformation. *Scripta Materialia*, 63(9):949–952, November 2010.

[83] T. S. Van Erp, T. P. Caremans, C. E. A. Kirschhock, and J. A. Martens. Prospects of transition interface sampling simulations for the theoretical study of zeolite synthesis. *Physical Chemistry Chemical Physics*, 9(9):1044–1051, 2007.

[84] E. Vanden-Eijnden and F. A. Tal. Transition state theory: variational formulation, dynamical corrections, and error estimates. *The Journal of Chemical Physics*, 123(18):184103, November 2005.

[85] E. Vanden-Eijnden and M. Venturoli. Revisiting the finite temperature string method for the calculation of reaction tubes and free energies. *The Journal of Chemical Physics*, 130(19):194103, 2009.

[86] T. Vegge, T. Rasmussen, T. Leffers, O. B. Pedersen, and K. W. Jacobsen. Determination of the of rate cross slip of screw dislocations. *Physical Review Letters*, 85(18):3866–3869, October 2000.

[87] G. Vineyard. Frequency factors and isotope effects in solid state rate processes. *Journal of Physics and Chemistry of Solids*, 3(1-2):121–127, 1957.

[88] L. Wang, J. Zhou, Y. Liu, Y. Zhang, S. andWang, and W. Xing. Nanovoid growth in nanocrystalline metal by dislocation shear loop emission. *Materials Science and Engineering: A*, 528(16-17):5428–5434, June 2011.

[89] D. H. Warner and W. A. Curtin. Origins and implications of temperature-dependent activation energy barriers for dislocation nucleation in face-centered cubic metals. *Acta Materialia*, 57(14):4267–4277, August 2009.

[90] D. H. Warner, W. A. Curtin, and S. Qu. Rate dependence of crack-tip processes predicts twinning trends in f.c.c. metals. *Nature Materials*, 6(12):1004, November 2007.

[91] M. Wen. Atomistic simulation of kink-pairs of screw dislocations in body-centred cubic iron. *Acta Materialia*, 48(17):4255–4265, November 2000.

[92] E. Wigner. The transition state method. *Trans. Faraday Soc.*, 34:29–41, 1938.

[93] K. J. Zhao, C. Q. Chen, Y. P. Shen, and T. J. Lu. Molecular dynamics study on the nano-void growth in face-centered cubic single crystal copper. *Computational Materials Science*, 46(3):749–754, September 2009.

[94] T. Zhu, J. Li, A. Samanta, A. Leach, and K. Gall. Temperature and strain-rate dependence of surface dislocation nucleation. *Physical Review Letters*, 100(2):025502, January 2008.

[95] T. Zhu, J. Li, and S. Yip. Atomistic study of dislocation loop emission from a crack tip. *Physical Review Letters*, 93(2):025503, July 2004.